AD-752 199

METHODS AND DESIGN OF SIMPLE DEVICES FOR ON-BOARD AND GROUND-BOUND ORBIT DETERMINATION

Daniel H. Jean

Air Force Institute of Technology
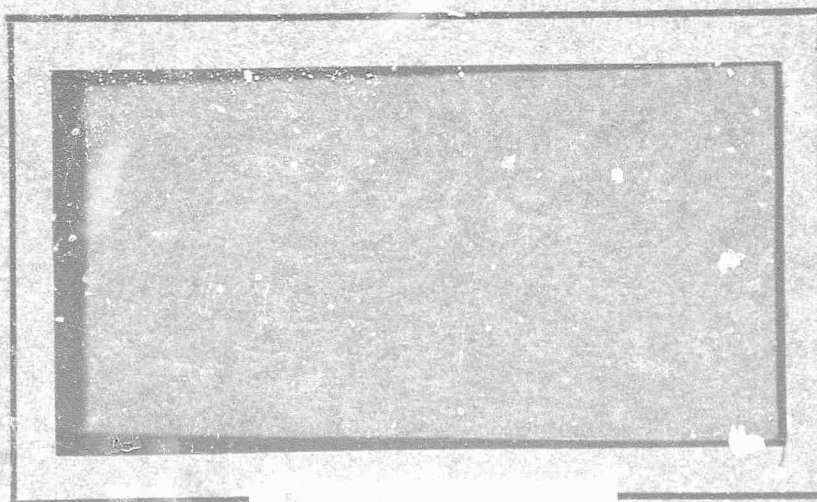Wright-Patterson Air Force Base, Ohio

June 1971

AIR FORCE INSTITUTE OF TECHNOLOGY

AIR UNIVERSITY
UNITED STATES AIR FORCE

SCHOOL OF ENGINEERING

WRIGHT-PATTERSON AIR FORCE BASE, OHIO

METHODS AND DESIGN

OF SIMPLE DEVICES FOR ON-BOARD

AND GROUND-BOUND ORBIT DETERMINATION

THESIS

GA/MC/71-1   Daniel H. Jean
             Major   USAF

Approved for public release; distribution unlimited.

METHODS AND DESIGN

OF SIMPLE DEVICES FOR ON-BOARD

AND GROUND-BOUND ORBIT DETERMINATION

THESIS

Presented to the Faculty of the School of Engineering

of the Air Force Institute of Technology

Air University

in Partial Fulfillment of the

Requirements for the Degree of

Master of Science

by

Daniel H. Jean, B.S.

Major   USAF

Graduate Astronautical Engineering

June 1971

Preface

Literature on the many methods of manual orbit deter-
mination is extensive as one might expect. However, in
the course of my research for simple computational methods
and devices, I noted that the graphical device known as a
velocity hodograph had virtually disappeared from recent
literature. I felt and still feel that the velocity hodo-
graph offers interesting possibilities for solving orbit
determination problems. To a large extent, this thesis is
devoted to practical applications of the velocity hodo-
graph. Since this graphical device incorporates the basic
concepts of orbital mechanics, I claim no truly original
ideas.

I would like to take this opportunity to express my
appreciation to Professor Peter Bielkowicz for leading me
through several courses in astrodynamics, suggesting this
topic, and finally, but certainly not least, for his
guidance and criticism during the writing of this thesis.
I also wish to acknowledge my gratitude to Captain Tony
Barth of the USAF Avionics Laboratory for providing me
with many research documents. My special thanks to my
family for their understanding and encouragement during
the preparation of this report, with particular expres-
sions of appreciation to my wife, Evelyne, for her

assistance in typing.

Daniel H. Jean

Details of illustrations in
this document may be better
studied on microfiche.

Contents

Contents

List of Figures

List of Figures

Abstract

Simple non-electrical methods and devices for orbit determination on the basis of explicit navigation are examined. Principal measuring devices discussed are the sextant, stadimetric instruments, and almucanters. Computational methods for solving the geometric orbital parameters are focused on adaptations of the velocity hodograph. Discussion includes sample problems and a general analysis of inherent errors.

METHODS AND DESIGN

OF SIMPLE DEVICES FOR ON-BOARD

AND GROUND-BOUND ORBIT DETERMINATION

I. Introduction

Background

After a decade of successful space exploration in the
vicinity of the earth which was climaxed by the Apollo
landing on the Moon, man continues to strive to penetrate
deeper into space. Of particular interest among possible
future manned missions are fly-bys and landings on other
near and distant planets of the solar system. Due to the
great distances involved, Earth-based radio navigation
capabilities will be severely limited if for no other rea-
son than time-delayed communication. Intuitively, this
situation leads to an emphasis on developing on-board
navigation procedures and measuring devices which are
totally independent and self-sufficient with respect to
collection of data (the observables) and orbit computa-
tions. In addition, missions landing on some planets may
be faced with determining the orbits of probes or command
modules from observations made on the ground. The method
which presents the greatest reliability, although not
necessarily the greatest accuracy, is most often the one
divorced from sophistication. Since electronic equipment

failure is a distinct possibility, simple non-electrical devices augmented by manual calculation schemes which are most general in applicability should be considered.

Problem

This report is intended to present a discussion of methods and design of simple devices for on-board navigation and ground level orbit determination, even in the event of electronic equipment failure. "On-board" navigation is defined as space navigation, the art of describing the spacecraft state from observables as seen from within the spacecraft, without resort to outside communication. "Ground based orbit determination" is defined as the art of describing a spacecraft state from observables as seen from the ground. The term "state" is defined as the position and velocity relative to some reference coordinate frame for a particular point in time. Classically, the state is expressed by a set of numerical constants called orbital parameters when the motion of the vehicle is in a free-fall trajectory.

Scope

Previous theses dealing with manual navigation were written by Captains Schehr and Smith ("Manual Astronaut Navigation: Apollo Mission Application") and by Major Horrigan and Captain Walsh ("Manual Astronaut Navigation") under the sponsorship of Professor Bielkowicz. These

gentlemen developed the Delta-H method which was initially applicable to small range, low-eccentricity orbits and then extended to highly eccentric elliptical orbits. In addition, these theses, combined together, form a wonderful synopsis of the measurements which can be made with a hand-held sextant or stadimeter and the computations which follow to specify the orbital parameters.

Rather than repeating their voluminous information in new or disguised verbage, the principle objective is to investigate simple non-electrical devices which can be used to collect observable data and the promising manual methods of calculation using the velocity hodograph.

Assumptions

The primary assumption made is that the spacecraft follows unperturbed, pure Keplerian flight. This implies that:

1. The trajectory is restricted to two-body motion and describes conic sections.

2. The gravity field of the attracting body is uniform, inverse-square, and central.

3. The mass of the spacecraft is negligible compared to the attracting body mass.

4. The vehicle is always considered to be located in one clearly defined space of influence such that travel from one body to another involves patch conic solutions.

3

Other assumptions made are that there are no pre-calculated reference trajectories which therefore implies relying on explicit navigation schemes, and that the reader is acquainted with the basics of orbital mechanics.

Organization

Chapter II deals with the design of simple devices used to measure the observables from a space vehicle.

Chapter III presents a theoretical discussion of the velocity hodograph.

Chapter IV provides examples of typical problems and their solution.

Chapter V deals with ground level orbit determination and associated hardware.

II. <u>Simple</u> <u>Measuring</u> <u>Devices</u>

Introduction

Space navigation as well as ground level orbit deter-
mination are both an instrumentation and computational
problem. All instrumentation and computational modes
should employ the same navigation concept. The concept
selected in this report is the "explicit" navigation
scheme. Explicit navigation is more desirable in the
sense that it can handle any situation which calls for a
deviation from the flight plan (Ref 12:428). Although
the explicit navigation method has the disadvantage of a
large computational load, it has the primary advantage of
providing the navigator with direct data on spacecraft
position and indirectly the velocity. The raw data that
must be obtained for use in the computations are position
fixes. The position fix data includes a radial line of
position (LOP) from the attracting body and a radial dis-
tance on the LOP. Three position fixes permit the naviga-
tor to fully define the orbit. Partial fixes which
include only the LOP or the radial distance can also
establish the orbital parameters completely or partially
depending on the conditions and circumstances; for example,
having only three ranges would only allow computing three
orbital parameters (See Chapter III for more details).

5
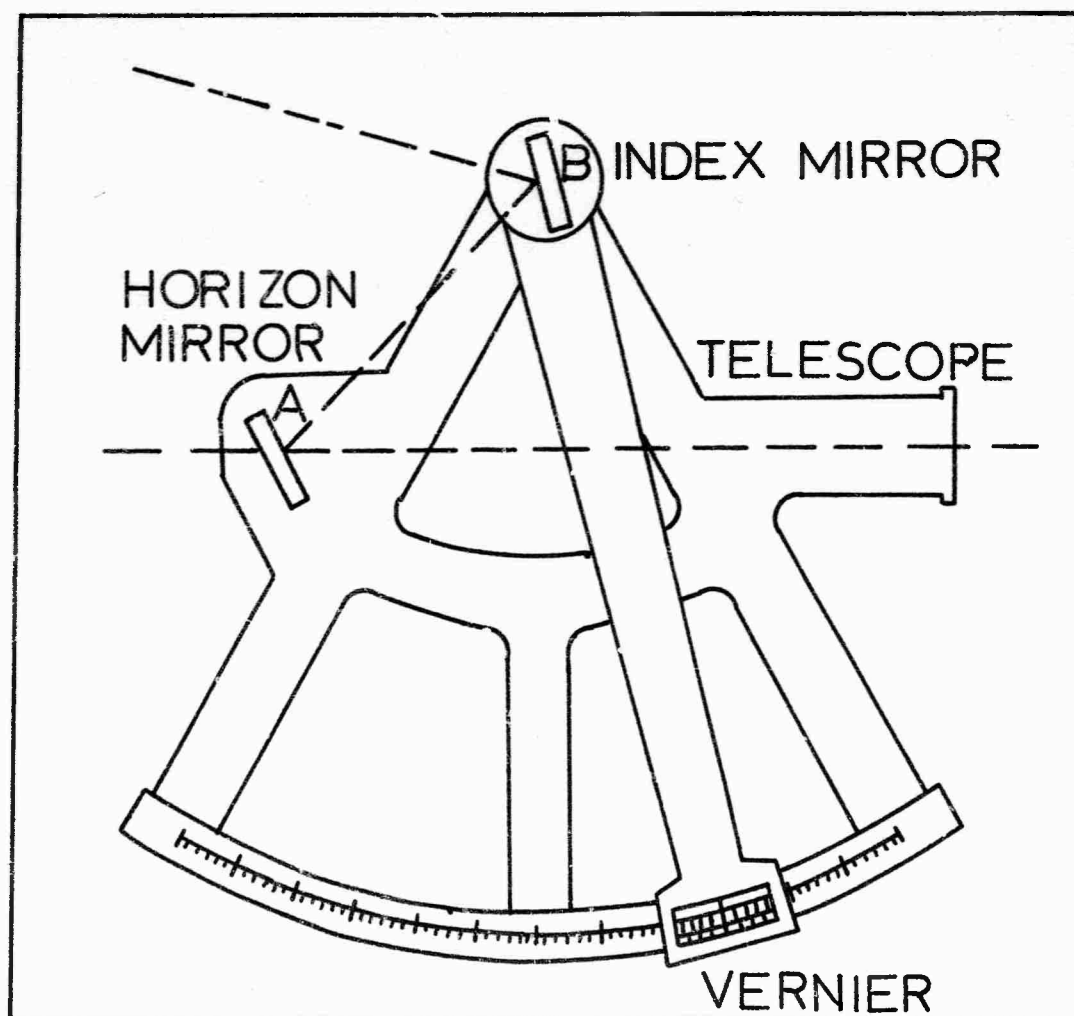
Figure 1. The Sextant

The types of non-electrical instruments that can provide LOP and range (radial distance) information are all optical instruments. Fortunately, the sighting and aiming involved is one area where the superior capabilities of the human eye for resolution and recognition can be used advantageously. Discussion of the individual instruments now follows.

The Sextant

The sextant is an instrument fitted with moving mirrors and prisms. The basic measurements taken are angles between the line-of-sight of one reference body to another, or to measure the angle subtended by the diameter of an apparent disc such as the sun, moon, or planets.

Oddly enough, the ancient mariner's sextant (Fig. 1) is readily adaptable, in principle, to space navigation and orbit determination problems. This adaptability was dramatically demonstrated during the manned space flights of Gemini IV, VII, and XII.

The required accuracy of sightings for lunar or planetary missions is several seconds of arc (Ref 4:208). Current marine sextants such as the Navy Mark II Mod 0 weights approximately 2.7 pounds. The vernier readout least count is 0.1 minute of arc (Ref 9:3). Although it is a well known fact that simply increasing the radius of the sextant arc will correspondingly increase the instrument accuracy, the limitations placed on weight, size,
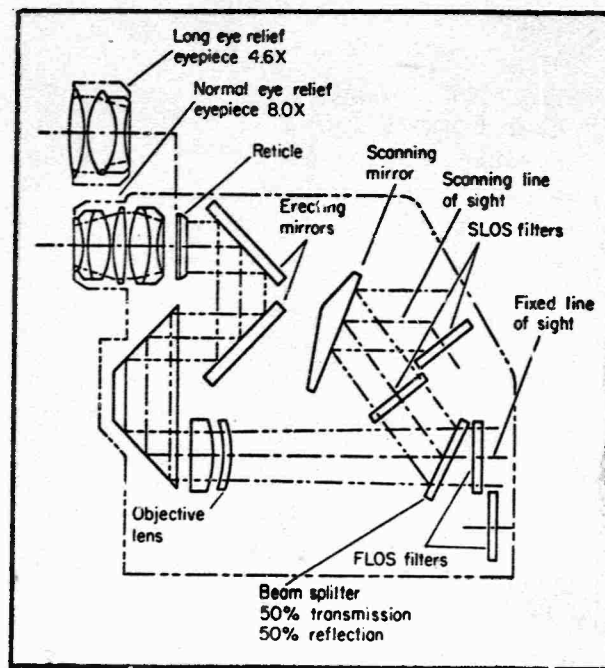
Figure 2. Schematic Diagram of
Optics; Hand-held
Sextant
(From Ref 20:4)

restricted field of view, and cramped quarters in the
current space program makes instrument accuracy purely an
engineering problem. Thus, the simple sextant becomes a
sophisticated piece of hardware containing such items as
precision stainless steel worm and worm wheels (35 mil-
lionth of an inch) and beryllium structural elements (Ref
14:198). The complexity may be easily visualized by
glancing at Figure 2.

Studies made at the NASA Ames Research Center,
Moffett Field, California, showed that the ability of
sextant operators to make accurate navigation measurements

8

was critically dependent of training. Test results at the
research center also indicated that increasing the sextant
telescope magnification from 2 to 20 power decreased the
average standard deviation from 22 seconds of arc to about
5 arcsec. The results of Gemini XII showed that hand-held
sextant performance was excellent, providing a standard
deviation measurement error of less than ± 10 arcsec (Ref
19:655).

A photographic sextant that can make conventional
sextant measurements and simultaneously provide positive
means for target star identification was also investigated
at the Ames Research Center. The summary of the study
concluded that the film was the most critical factor and
that currently available emulsions lack either resolution,
speed, or ease of development (Ref 24:1).

The Stadimeter

The stadimeter is a device used to obtain the dis-
tance separating the observer from another body by taking
angular measurements of that body and provided the body's
diameter is known. There are two classes of systems:
systems viewing a limited portion of the target and sys-
tems viewing the entire target.

Development of the stadimeter by the U.S. Air Force
and the Kollsman Instrument Corporation has emphasized
the class of instruments measuring the amount of curvature
evident in the limited field of view available. The

9

observed curvature can be translated into range by means of precomputed calibration curves. One way to obtain the curvature is to measure the deviation angle between two chords connecting three equidistant horizon points (A, B, and C). A pair of composite prisms creates three super-imposed fields of view. The deviation angle is measured when the three arcs of the horizon intersect (Fig. 3). Another method consists of a triple split image field with a center scanning prism (Fig. 4) which when aligned with the outer segments 1 and 3, the angle θ can be read directly from the stadimeter.

The equation providing the relationship between the measured angle θ and the altitude h as geometrically presented in Figure 5 is

$$h = R \left\{ \frac{\sqrt{1 - \left(\frac{\cos \frac{A}{2} \cos \theta' - \cos^2 \frac{A}{2}}{1 - \cos \frac{A}{2} \cos \theta'} \right)^2}}{\sin \frac{A}{2}} - 1 \right\} \qquad (2\text{-}1)*$$

where

R = radius from body center to horizon

A = fixed angle between the side lines of sight

θ' = measured angle θ plus a correction angle $\delta\theta$

The pre-computed calibration curves plot h versus θ; however, from Eq (2-1) it is evident that (h/R) versus θ' can

*This equation is derived in Ref 18:117.

HORIZON

CHORDS TO THE HORIZON

β

arc length $\widehat{AB}$ = arc length $\widehat{BC}$

β = the measure of curvature

INSTRUMENT FIELD OF VIEW

RETICLE CROSS LINE

1.

2.

3.
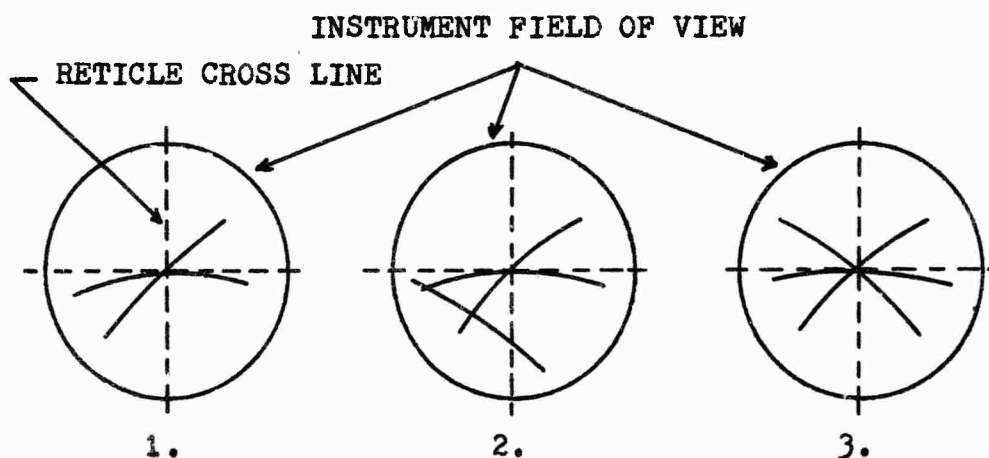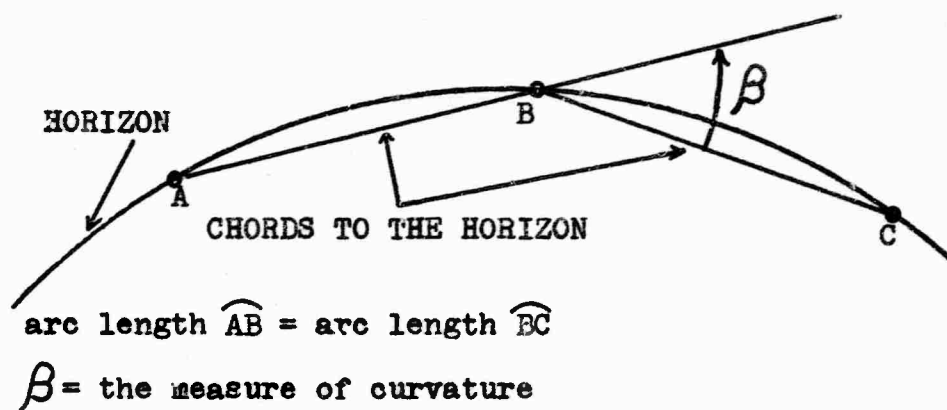
1. Stadimeter pointed at horizon so that the images of the horizon at A and B cross horizon at C out of the field of view.

2. Horizon at C brought into field of view.

3. Horizon at C aligned upon the intersection of the horizons at A and B. The reticle aids in this operation.

Figure 3. Horizon Geometry and Alignment of Images in Instrument Field of View (From Ref 25:8-9)
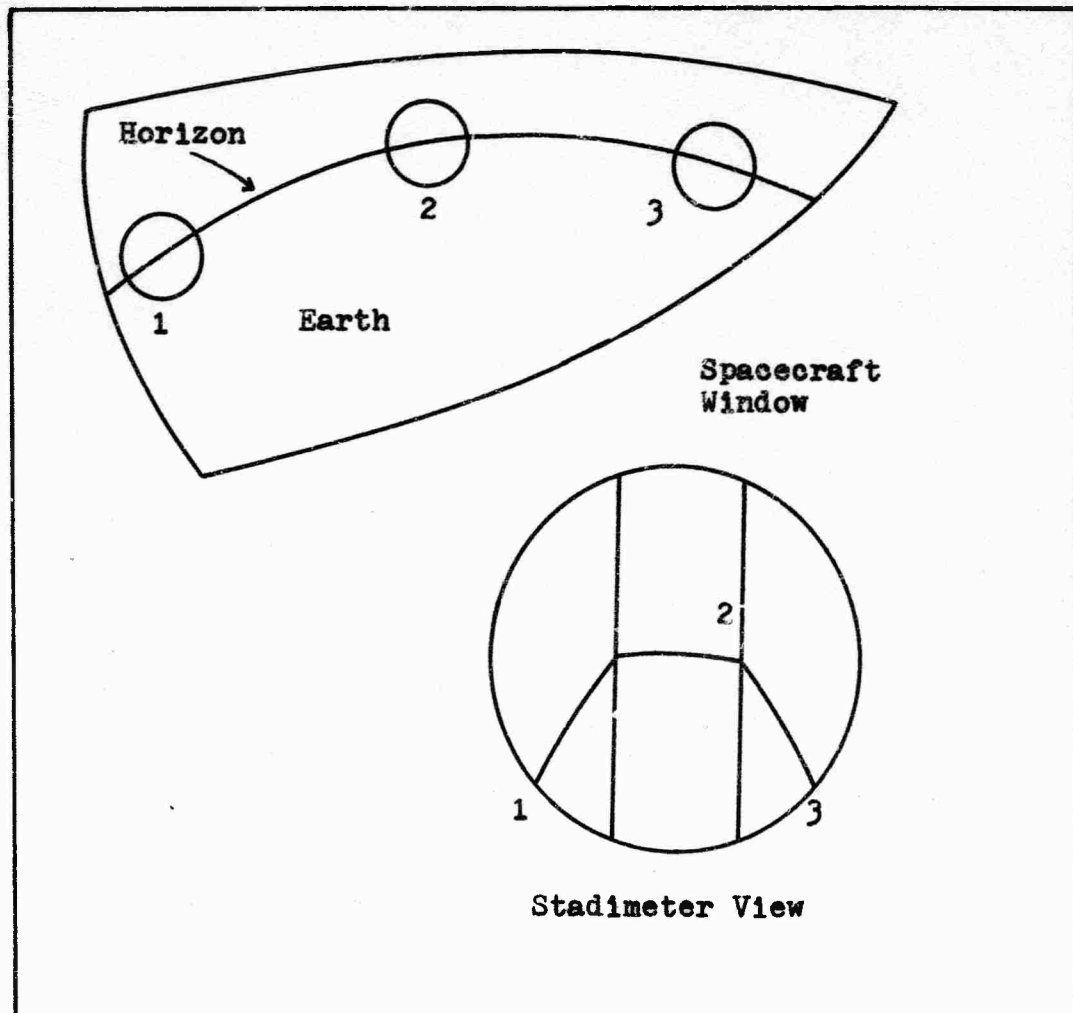
Figure 4. Stadimetric View
(From Ref 13:102)

Figure 5. Geometry of Stadimetric Measurement
(From Ref 13:103)

also be plotted. Since θ and $\delta\theta$ are both dimensionless functions of R and h, a plot of (h/R) versus θ would be more general since it would apply to any heavenly body (See Appendix A for specific relatioships).

The stadimeters just discussed are intended for use at low altitudes. For example, the USAF Space Stadimeter is not intended for use above 2500 NM altitude. For spacecraft altitudes above 2500 NM, the angular diameter of the body can be measured (Fig. 6). The following

Figure 6. Stadimetric Angle With Respect
to a Spherical Body

equation is used to determine range

$$r = \frac{d/2}{\sin \psi/2} = \frac{R}{\sin \psi/2} \qquad (2\text{-}2)$$

where

        d = diameter of body

        ψ = angle subtended over diameter

The second class of stadimeters views the entire
target. A typical method is one proposed by L.M. Vorob'ev
(Ref 23:126) which consists of a movable circular screen
(Fig. 7) whose plane is perpendicular to the direction of
the celestial body. The screen of diameter 2r moves per-
pendicularly to the axis 00, to a position where the edges
of the celestial body are barely visible. The subtended
half angle from Figure 7 is

14
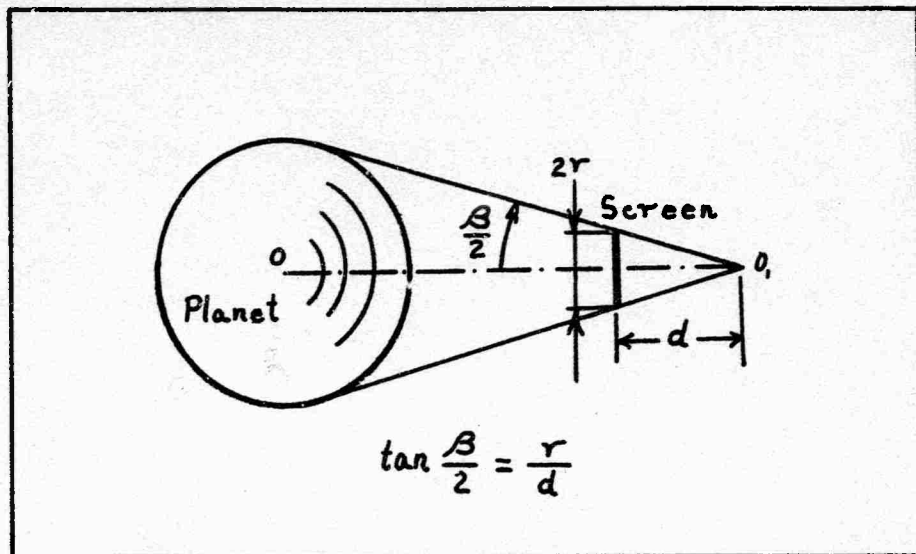
Figure 7. Measurement of the Angular
Diameter β of a Planet
By Means of a Movable
Circular Screen of Radius r
(From Ref 23:126)

$$\frac{\beta}{2} = \arctan \frac{r}{d} \qquad (2\text{-}3)$$

Substituting the value for the planet radius and the
angle $\beta/2$ into Eq (2-2) produces the range value.

Zenith Viewing Telescope

A simple optical instrument called a "bazooka" or
zenith viewing telescope as illustrated in Figure 8 can be
used to establish the local vertical of the spaceship
above the surface of the celestial body (Ref 16:289).

15
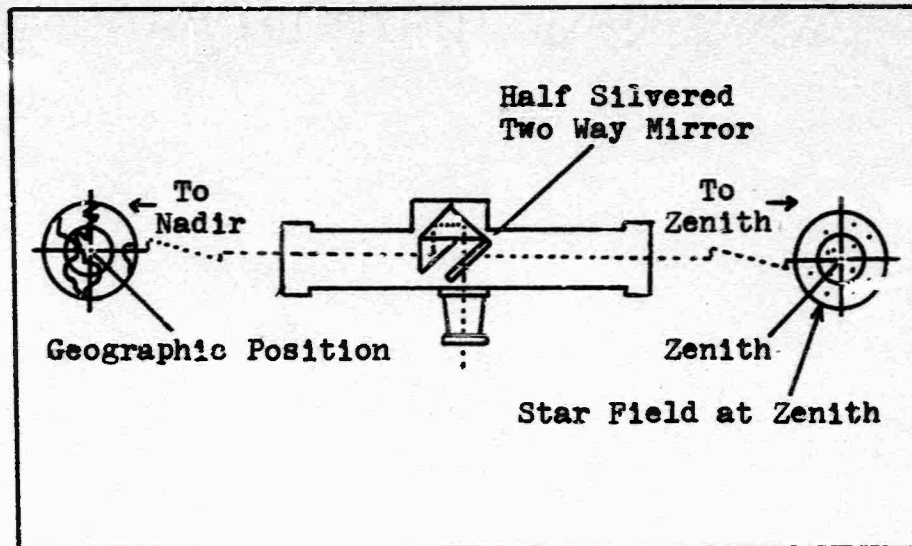
Figure 8. Zenith Viewing Telescope
(From Ref 26:790)

Theoretically, this method amounts to star-matching. An
identified star at the zenith would immediately establish
the line of position in terms of right ascension and
declination.

The Almucantar

The almucantar is a general application of the
"bazooka" telescope. This system calls for establishing
a local vertical vector which is the symmetric axis for
cones whose semi-angle is measured from the zenith. Thus
a simple peep sight centering element placed at the cone
apex and concentric circles scribed on a window with the
zenith at the center would theoretically suffice (Ref 10:
249). The concentric circles represent degrees of co-alti-
tude. Knowing the co-altitude of two stars at any instant

of time can establish a LOP, (assuming that the navigator can eye ball the zenith to resolve any ambiguity).

Angular Accuracy

In reality, any parameter is measured with some error. Besides the usual instrumentation and personnel error, such factors as the aberration of light, confusion with binary stars, and proper motion of stars can contribute to erroneous measurements.

Aberrational displacement due to the spacecraft's velocity is small for velocities of 10 to 20 km/sec but for velocities of about 100 km/sec, the angular displacement may approach 1 minute.

The distance between components of binary stars are relatively large. For example, the components of the binary star in Ursa Major are situated about 12' apart (Ref 23:125). The best solution for alleviating this error is to avoid using binary stars.

Proper motion of stars can be dismissed on the assumption that the star catalog in use is current and that the annual proper motion of stars is measured in microradians.

The effect of angular measurement error increases with the distance from the body. For example, a space vehicle situated approximately 80 million miles from the sun and 20 million miles from each of two planets being sighted, a total error of 30 arcsec would result in a 12,000 mile error in position, in a direction perpendicular to a line

to the sun and about 3,000 miles in directions perpendic-
ular to lines connecting the vehicle with the planets
(Ref 8:39).

Range Accuracy

From Eq (2-2) it is evident that for a given angular
error δ and a given body radius R that the range error is
magnified as the range increases.

The more difficult error to handle is the one con-
cerning the body radius. Errors in body radius measure-
ment are attributable to the influence of the planets'
atmospheres and their nonsphericity. To a great extent
the former reason is due to a question of definition.
For example, the radius of the Earth for stadimetric meas-
urements is taken as the airglow radius which is 14.9 NM
above the average earth surface radius. Since, as previ-
ously mentioned, this error is due to definition it will
not be discussed further.

Looking at the non-sphericity problem, the assumption
may be made that if the body is not a sphere then it is an
ellipsoid of revolution about its spin axis. Just as it
is necessary to know the radius of a spherical body, here
the oblateness must also be known; therefore, let it be
assumed that the following physical characteristics of the
planet are common knowledge

a = semi-major axis

b = semi-minor axis

18

e = planet eccentricity

Since the planet is like a spinning top or gyro, the intercept of the celestial sphere by the axis is fixed in space and can be identified or at least nearly approximated by some star. For example in Figure 9, the intercept is labeled as Star Q. Angle δ is the smallest or largest angle measured from Star Q to the body surface in the XY plane or any other plane containing the spin axis. Looking at the ellipsoid from a great distance the body appears as a circle of radius a when $\delta = 180^\circ$ and it appears as an ellipse with a semi-minor axis equal to b when $\delta = 90^\circ$. In fact, from any intermediate angle δ, the body seen from a great distance such as at point A appears as an ellipse whose semi-minor axis R is

$$R = a \left(1 - e^2 \sin^2 \delta \right)^{\frac{1}{2}} \qquad (2\text{-}4)$$

Note that R is also the apparent radius of the body measured in the XY plane. The point of tangency is A°, but a perpendicular constructed from the line-of-sight APA' to the body center is R, (the apparent radius as viewed from point A).

At point P the angles δ_1 and δ_2, or δ_1 and ϕ, may be measured with a sextant and the sliding screen stadimeter. R_1 and R_2 can be calculated from Eq (2-4). Since ϕ is the difference between δ_1 and δ_2, suppose that δ_1 and ϕ are the angles measured. From the problem geometry

19
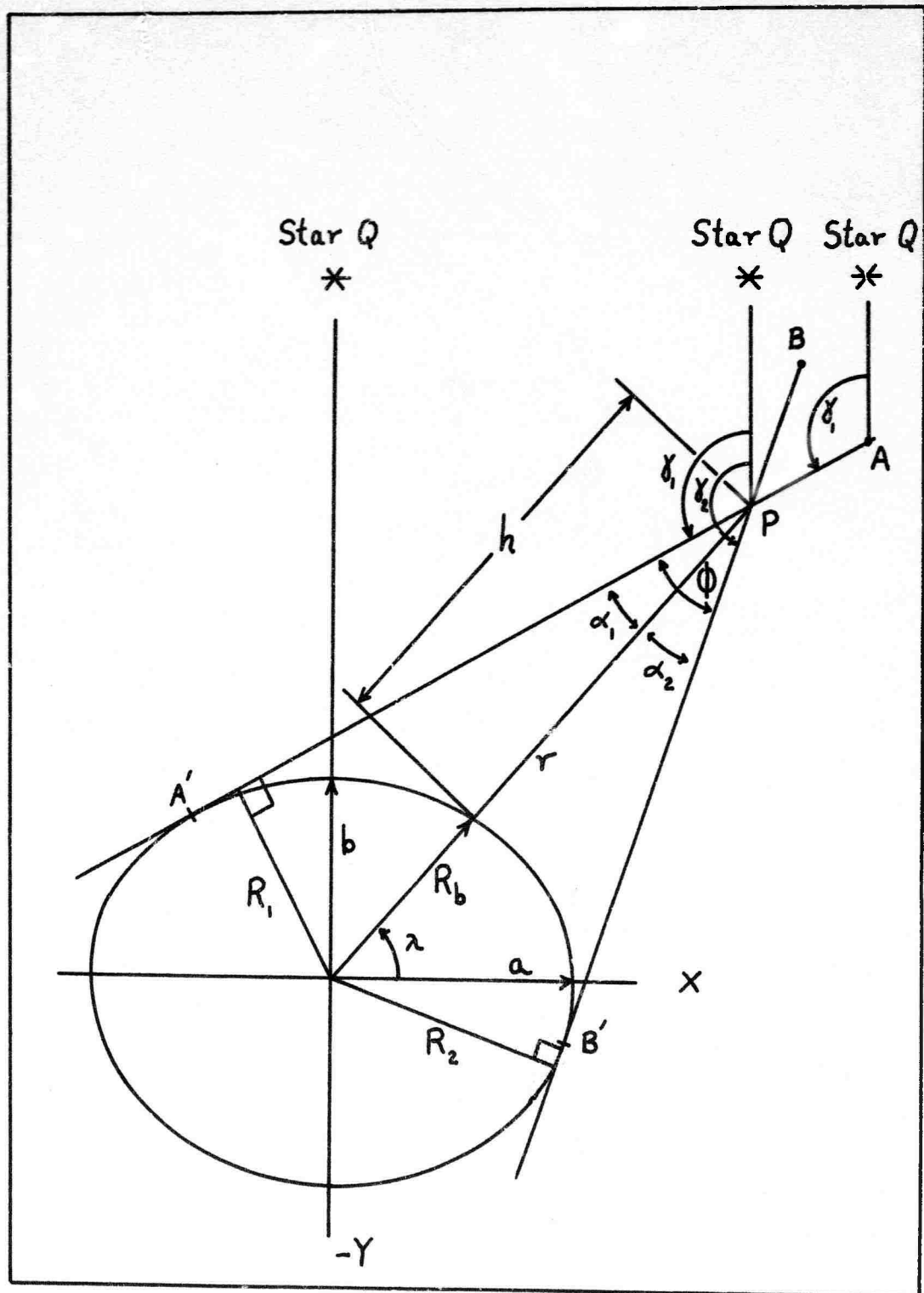
Figure 9.   Geometry of Stadimetric
Viewing of an Ellipsoid

$$r = R_b + h = \frac{R_1}{\sin \alpha_1} = \frac{R_2}{\sin (\phi - \alpha_1)} \qquad (2\text{-}5)$$

where

r = radial distance to vehicle

R_b = body surface radius on the line joining the body center and spacecraft

h = altitude

α_1 = subtended radius arc for the apparent radius R_1

Application of a trigonometric identity and rearranging Eq (2-5) yields

$$\frac{\sin \phi \cos \alpha_1 - \cos \phi \sin \alpha_1}{\sin \alpha_1} = \frac{R_2}{R_1} \qquad (2\text{-}6)$$

therefore

$$\alpha_1 = \cot^{-1} \left[\frac{(R_2/R_1) + \cos \phi}{\sin \phi} \right] \qquad (2\text{-}7)$$

Having solved α_1, let $\psi/2 = \alpha_1$ and substitute into Eq (2-2) to obtain the range r.

The angle λ which corresponds to the body latitude may be found from the following equation

21

$$\lambda = 180° - (\gamma_1 + \alpha_1) \qquad (2\text{-}8)$$

Knowing λ, the body radius R_b on the line connecting the body center with the spacecraft is

$$R_b = \frac{ab}{\left(a^2 \sin^2\lambda + b^2 \cos^2\lambda\right)^{1/2}} \qquad (2\text{-}9)$$

and the altitude can be immediately obtained from Eq (2-5).

As just shown, the problem of non-sphericity can be handled through additional calculations so that oblateness need not introduce range errors. Thus, the accuracy in range is really dependent on how well the physical dimensions of a celestial body are known.

I.:.. The Velocity Hodograph

Introduction

Graphical solutions can be developed advantageously in the solution of problems in space flight. Graphs are pictures, which, as is so often said, are worth a thousand words. It geometrically portrays numerical results that are mathematically difficult to grasp. The velocity hodograph defined as the locus of velocity vectors is a geometrical picture which reduces all conic sections to mapped circles.

Mathematical Derivation

If motion of the spacecraft is described in polar coordinates, the velocity vector can be defined by two orthogonal components: the radial velocity, $\dot{r}$, and the transverse velocity, $r\dot{\theta}$. The equations used to develop the hodograph equation are

$$V^2 = \dot{r}^2 + \left(r\dot{\theta}\right)^2 = \mu\left(\frac{2}{r} - \frac{1}{a}\right) \qquad (3-1)$$

$$h^2 = \mu\left[a\left(1 - e^2\right)\right] \qquad (3-2)$$

$$h = r^2\dot{\theta} = constant \qquad (3-3)$$

23

where

a = semi-major axis

e = eccentricity

h = angular momentum per unit mass

V = total velocity

r = radial distance

$\dot{\theta}$ = angular velocity

μ = gravitational constant

Substituting Eq (3-3) into (3-2) and rearranging yields

$$\frac{1}{a} = \frac{\mu(1 - e^2)}{h^2} \qquad (3-4)$$

Eq (3-4) can now be directly substituted into Eq (3-1) to give

$$\dot{r}^2 + (r\dot{\theta})^2 = \mu\left[\frac{2}{r} - \frac{\mu(1 - e^2)}{h^2}\right] \qquad (3-5)$$

which when rearranged yields Eq (3-6) below. It is immediately recognized as the equation of a circle with coordinate axes $\dot{r}$ and $r\dot{\theta}$. It should be noted that in the preceeding development the initial equations, Eq (3-1) and Eq (3-2), are equations for circular and elliptical sections; however, the same resulting equation is produced assuming parabolic or hyperbolic conic sections.

$$\dot{r}^2 + \left(r\dot{\theta} - \frac{\mu}{h}\right)^2 = \left(e\frac{\mu}{h}\right)^2 \qquad (3-6)$$

24

Eq (3-6) as notated represents a graph with a "float-
ing" center. It is desirable to fix the center such that
a pre-plotted graph can be constructed and used under all
circumstances. This can be accomplished by reducing the
equation to a non-dimensional form. Thus, dividing Eq
(3-6) by $(\mu/h)^2$ yields

$$\left(\frac{\dot{r}h}{\mu}\right)^2 + \left(\frac{r\dot{\theta}h}{\mu} - 1\right)^2 = e^2 \qquad (3-7)$$

Letting

$$X = \frac{r\dot{\theta}h}{\mu} = \frac{r^3\dot{\theta}^2}{\mu} \qquad (3-8)$$

and

$$Y = \frac{\dot{r}h}{\mu} = \frac{\dot{r}\,r^2\dot{\theta}}{\mu} \qquad (3-9)$$

it is evident that in the X,Y coordinates the origin for
circles of radius e is centered at the point (1,0) as
shown in figure 10.

Discussion

Many interesting relationships can be obtained by
just looking at X and Y, for example:

$$X = \frac{r\dot{\theta}h}{\mu} = \frac{r^3\dot{\theta}^2}{\mu} = \frac{(r\dot{\theta})^2}{V_{cc}^2} = \frac{h^2}{\mu r} = 1 + e\cos\theta \qquad (3-10)$$

25
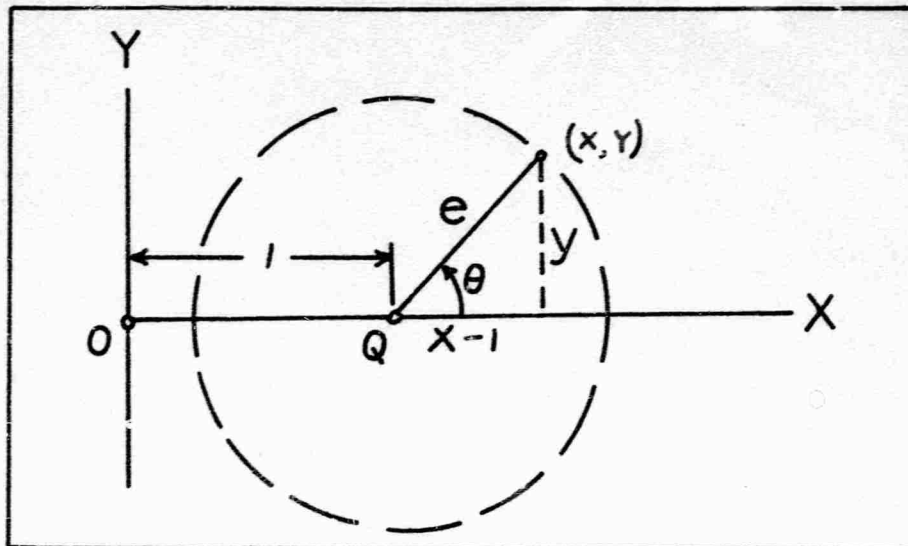
Figure 10. Dimensionless Polar
Hodograph of Velocity

and

$$Y = \frac{\dot{r}h}{\mu} = \frac{\dot{r}r^2\dot{\theta}}{\mu} = \frac{\dot{r}X^{\frac{1}{2}}}{V_{Lc}} = e\sin\theta \qquad (3\text{-}11)$$

where V_{Lc}, the local circular velocity, is $\sqrt{\frac{\mu}{r}}$. Obviously many more rearrangements are possible. From Eq (3-10) it becomes immediately apparent that θ is the true anomaly and since X is equal to (1+e) when θ is zero and $(r\dot{\theta})$ is maximum, it follows that the point (1+e,0) is the perifocal point. By the same type of argument (1-e,0) is the apofocal point; however, it should be noted from Eq (3-8) that points where X is equal to or less than zero are not physically defined. Furthermore, it should be noted that the X axis represents the apsidal axis. As the true anomaly increases from perifocal point, $\dot{r}$ is always initially

26

positive so from Eq (3-11) it is deduced that θ is meas-
ured in the counterclockwise direction since Y is initial-
ly positive.

Additionally, it is evident that the arctangent of
(Y/X) is the same as $(\dot{r}/r\dot{\theta})$ so that a line joining point 0
to point (X,Y) forms an angle with the X axis equal to the
flight path angle.

Time from peripoint passage can be indirectly obtain-
ed by adding new curves to the graph. Consider the time
equations (Ref 2:4-5) for an ellipse,

$$\Delta t = \left(\frac{a^3}{\mu}\right)^{1/2}\left\{2\,\tan^{-1}\left[\sqrt{\frac{1-e}{1+e}}\,\tan\frac{\theta}{2}\right] - e\sqrt{1-e^2}\,\frac{\sin\theta}{1+e\cos\theta}\right\} \qquad (3-12)$$

for a hyperbola,

$$\Delta t = \left(\frac{a^3}{\mu}\right)^{1/2}\left\{\left(e\sqrt{e^2-1}\right)\frac{\sin\theta}{1+e\cos\theta} - \ln\frac{\sqrt{e+1}+\sqrt{e-1}\,\tan\frac{\theta}{2}}{\sqrt{e-1}-\sqrt{e-1}\,\tan\frac{\theta}{2}}\right\} \qquad (3-13)$$

and for a parabola

$$\Delta t = \frac{h^3}{2\mu^2}\left(\tan\frac{\theta}{2} + \frac{1}{3}\tan^3\frac{\theta}{2}\right) \qquad (3-14)$$

Noting that

$$\left(\frac{a^3}{\mu}\right)^{\frac{1}{2}} = \frac{h^3}{\mu^2}\left|1-e^2\right|^{-\frac{3}{2}} \tag{3-15}$$

Eq (3-12), (3-13), and (3-14) can be written as

$$\Delta t = K\frac{h^3}{\mu^2} = KrX\sqrt{\frac{rX}{\mu}} \tag{3-16}$$

where $K = f(e, \theta)$, thus

$$K = 0 \qquad \text{for } \theta = 0^\circ$$
$$K = \pi\left(1-e^2\right)^{-\frac{3}{2}} \qquad \text{for } \theta = 180^\circ$$

By preplotting constant lines of K (Ref 3:13), time may be computed from Eq (3-16). The time so obtained is normally expressed in the units used in the gravitational constant μ (See Fig. 11).

The range (radial distance) at any point on the free-fall trajectory can be easily found after one point of the orbit's eccentricity circle is associated with a range value. Knowing range r_1 at point (X_1, Y_1) the square of the angular momentum per unit mass is obtained from Eq (3-10)

$$h^2 = r_1\mu X_1 \tag{3-17}$$

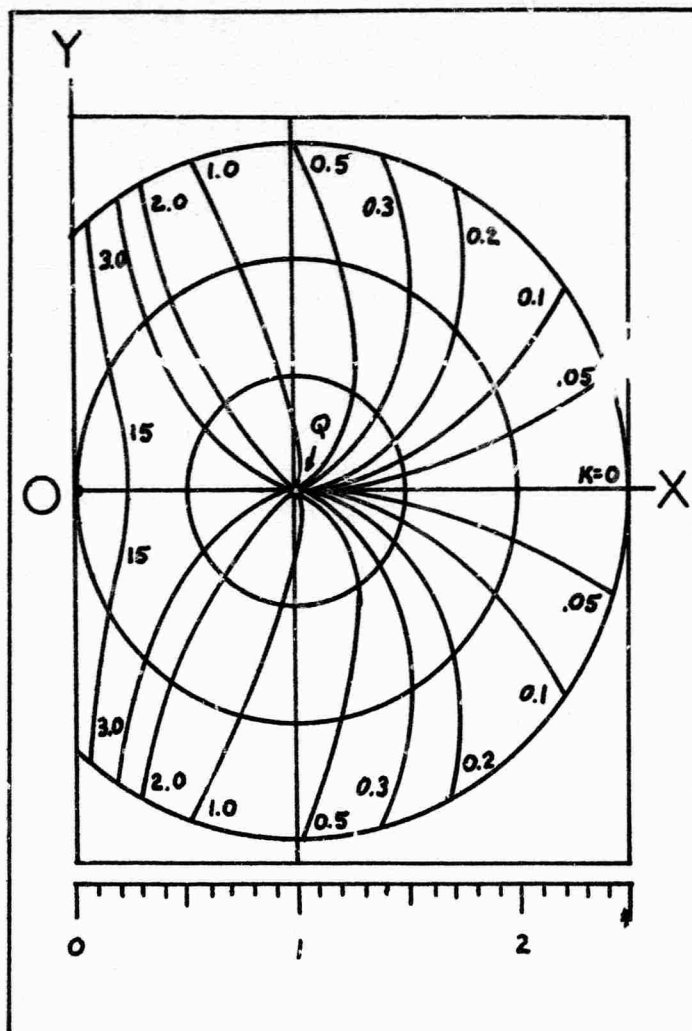The second point fixes X_2 and by the conservation of angular momentum

28

Figure 11. Time Lines of Constant K
(From Ref 5:39)

$$r_2 \, \mu X_2 = r_1 \, \mu X_1 \qquad (3\text{-}18)$$

Thus the calculated range is

$$r_2 = \frac{r_1 X_1}{X_2} \qquad (3\text{-}19)$$

29

It follows that the peripoint radial distance must be

$$r_p = \frac{rX}{1+e} \qquad (3\text{-}20)$$

The semi-major axis for all conics can be expressed as

$$a = \frac{rX}{|1-e^2|} \qquad (3\text{-}21)$$

The semi-latus rectum, p, is simply

$$p = rX \qquad (3\text{-}22)$$

Concept and Method of Graph Usage

In order to increase the accuracy of data extracted from the graphs it is evident that the graph must be quite large and have a dense grid of lines to minimize the errors associated with interpolation. Obviously, combining cartesian coordinates, polar coordinates, and time constant curves on one graph would be shear nonsense. Instead, it is suggested that there be three separate graphs plus a transparent overlay which would merely serve to transfer the plotted points from one graph to another.

As seen in Figure 12, the three graphs are the (X,Y) cartesian graph, the (e, θ) polar graph and the graph of time constant curves K. If the distances X = 1 and e = 1 are represented by a length of 20 centimeters, each graph
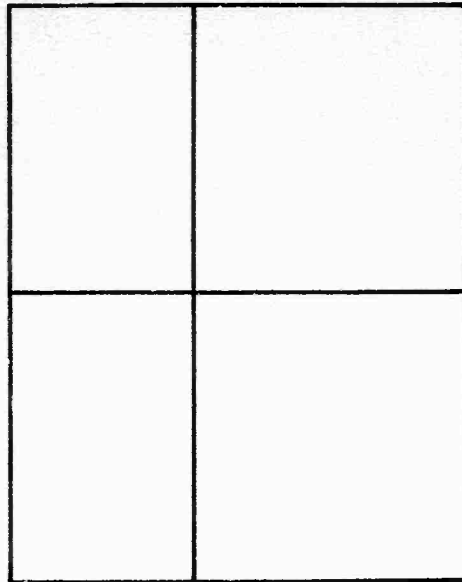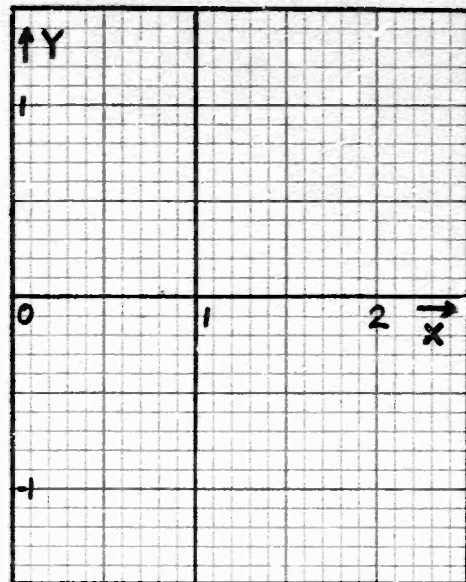
Transparent Overlay   X,Y Cartesian Coordinates
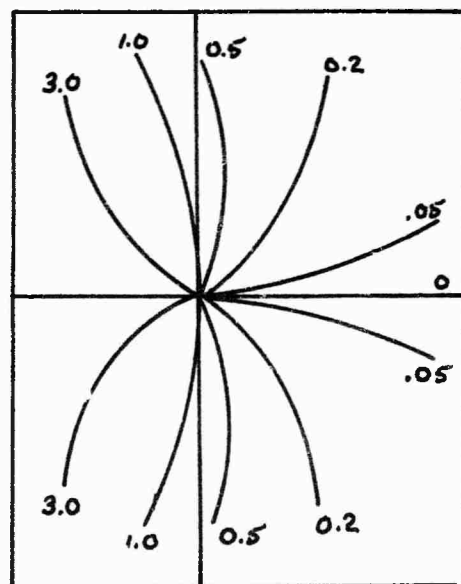
e,θ Polar Coordinates   Time Constant Curves, K

Figure 12. Composite Graphs

similar to those shown in Figure 12 would measure 50 cm horizontally by 60 cm vertically. Line intervals of 2 mm would provide X, Y and e scale readings to 0.01 without interpolation and to about 0.001 with interpolation. In addition, the cartesian and polar graphs have the potential to be contracted in scale by factors of ten in order to deal with orbits having an eccentricity less than 0.1.

Case Studies of Applicability to Orbit Determination

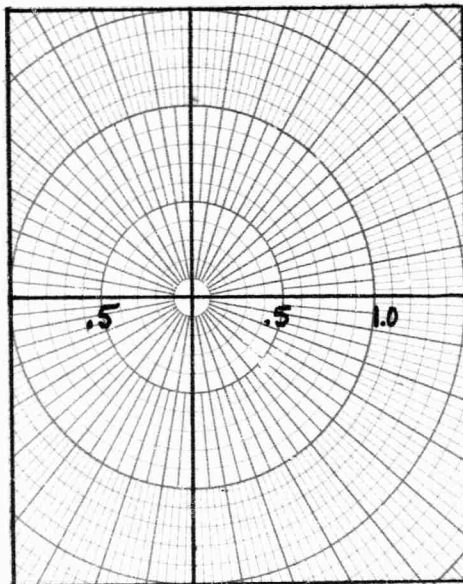For simplicity, let it be assumed that a set of three observations exists containing range r (i.e., radial distance from the center of the attracting body) and angular data ψ where ψ is the central body angle or great circle arc on the celestial sphere between the line-of-position 1 and the succeeding LOP's. The data is (r_1, ψ_1), (r_2, ψ_2), and (r_3, ψ_3). From the polar coordinate equation for conic sections, one can derive an expression for X and Y in terms r's and ψ's. (See Appendix E). With X, Y and r known the problem is essentially solved.

A second case can be considered where the angular measurements are not included. Here the data consists of (r_1, t_1), (r_2, t_2) and (r_3, t_3) where $t_1 < t_2 < t_3$. Using equal time intervals and numerical differentiation (See Appendix B), it is possible to determine $\dot{r}$ and $\ddot{r}$, but not $\dot{\theta}$ thus posing some difficulty. The difficulty is immediately resolved by substituting the following equation (See Appendix C)

$$\left(r\dot{\theta}\right)^2 = V_{LC}^2 + r\ddot{r} \qquad (3\text{-}23)$$

into Eq (3-10) producing the relationships

$$X = 1 + \frac{r^2\ddot{r}}{\mu} \qquad (3\text{-}24a)$$

or

$$X = 1 + \frac{r\ddot{r}}{V_{LC}^2} \qquad (3\text{-}24b)$$

where V_{LC} is the local circular velocity for radial distance r. Manipulation of Eq (3-10), and (3-11) yields

$$Y = \dot{r}\sqrt{\frac{rX}{\mu}} \qquad (3\text{-}25a)$$

or

$$Y = \frac{\dot{r}\sqrt{X}}{V_{LC}} \qquad (3\text{-}25b)$$

The solution for finding the geometric orbital parameters immediately follows.

The third case occurs when the following data is obtained: (θ_1, t_1), (r_2, θ_2, t_2) and (θ_3, t_3). Here, X can be found from Eq (3-8) and from the first time derivative of the angular momentum the following expression for $\dot{r}$ is given as

$$\dot{r} = -\frac{r\ddot{\theta}}{2\dot{\theta}} \qquad (3\text{-}26)$$

Having found r, Y can be solved so that knowing r, X, Y the problem is solved.

The final case is the situation where ranges cannot be obtained; only the angular measurements are available. The data consists of (θ_0, t_0), (θ_1, t_1), (θ_2, t_2), (θ_3, t_3), and (θ_4, t_4). It is now necessary to lean heavily on equations derived by Mssrs. R.H. Gersten and Z.E Schwarzbein (Ref 22:697). Their equations are:

$$e \cos\theta_1 = \widetilde{Q}/\widetilde{S} \qquad (3\text{-}27)$$

$$e \sin\theta_1 = \widetilde{R}/\widetilde{S} \qquad (3\text{-}28)$$

where

$$\widetilde{Q} = \left(\dot{\theta}_2\right)^{\frac{1}{2}} \sin\Delta\theta_{13} - \left(\dot{\theta}_3\right)^{\frac{1}{2}} \sin\Delta\theta_{12}$$

$$+ \left(\dot{\theta}_1\right)^{\frac{1}{2}} \left[\sin\Delta\theta_{12} - \sin\Delta\theta_{13}\right] \qquad (3\text{-}29)$$

$$\widetilde{R} = -\left(\dot{\theta}_3^{\frac{1}{2}} - \dot{\theta}_1^{\frac{1}{2}}\right) \cos\Delta\theta_{12}$$

$$+ \left(\dot{\theta}_2^{\frac{1}{2}} - \dot{\theta}_1^{\frac{1}{2}}\right) \cos\Delta\theta_{13}$$

$$- \left(\dot{\theta}_2^{\frac{1}{2}} - \dot{\theta}_3^{\frac{1}{2}}\right) \qquad (3\text{-}30)$$

$$\tilde{S} = \left(\dot{\theta}_1\right)^{\frac{1}{2}} \sin\left(\Delta\theta_{13} - \Delta\theta_{12}\right)$$
$$+ \left(\dot{\theta}_3\right)^{\frac{1}{2}} \sin\Delta\theta_{12} - \left(\dot{\theta}_2\right)^{\frac{1}{2}} \sin\Delta\theta_{13} \qquad (3\text{-}31)$$

$$\Delta\theta_{ij} = \theta_j - \theta_i \qquad (3\text{-}32)$$

From Eq (3-27) and (3-28) it is clear that

$$X = 1 + \tilde{Q}/\tilde{S} \qquad (3\text{-}33)$$

and

$$Y = \tilde{R}/\tilde{S} \qquad (3\text{-}34)$$

Although X and Y can be found, a range must be associated with the point (X,Y) in order to progress with the solution. An expression for range can be obtained from Eq (3-8); it is

$$r_1 = \left(\frac{\mu X}{\dot{\theta}_1^2}\right)^{\frac{1}{3}} \qquad (3\text{-}35)$$

With X, Y, and the corresponding range, r_1, known the problem is readily solvable.

Summary

The main advantage of the velocity hodograph is that by mapping all conic sections into circles a quick graphical method is provided for the determination of three

orbital parameters and other relationships. The orbital
elements are the eccentricity

e- read directly from graph

the semi-major axis

$$a = \frac{rX}{|1 - e^2|} \qquad (3-21)$$

and time to or from peripoint

$$\Delta t = K \, rX \sqrt{\frac{rX}{\mu}} \qquad (3-16)$$

Other relationships of interest that can be obtained are
the true anomaly

θ - read directly from graph

the radial distance at peripoint

$$r_\rho = \frac{rX}{1 + e} \qquad (3-20)$$

and the semi-latus rectum

$$\rho = rX \qquad (3-22)$$

Other advantages are that the hodograph is independ-
ent of the central body (i.e., it can be used when orbit-
ing any central body, hence, serves all planets and the sun)
and that it can be used to calculate guidance maneuvers
(Ref 21:905). No aspects of guidance are considered in
this thesis other than to state here and now that guidance

consists of orbital maneuvers based on conclusions gained from knowing the orbital parameters. Additional information can be obtained in references 1 and 21.

In the discussion of applicability it was shown that it is possible to obtain from range and angle, range only, and angle only data the information required to fix a point (X,Y) on the hodograph with an associated value of range.

IV. Sample Problems and Solutions

Introduction

Previously in Chapter II, the position fix consisting of a line-of-position (LOP) and a radial distance was discussed. The LOP is a line from the attracting body center through the spacecraft position and extended to the celestial sphere. The intersection of the LOP with the celestial sphere can be given in terms of Latitude δ and East Longitude α. Since the radius vector contained in the orbital plane traces an arc of a great circle on the celestial sphere, two orbital orientation parameters — inclination and right ascension — can be obtained using spherical trigonometry. Furthermore, knowing the true anomaly which can be found from the velocity hodograph, in addition to knowing the inclination and right ascension provides the necessary data to determine the argument of peripoint through more spherical trigonometry (See Appendix D). The three orbital parameters — inclination, right ascension, and argument of peripoint — will not be discussed in the following problems since the calculations must always be based on two LOP's and follow the same or comparable mathematics suggested in Appendix D. In the sample calculations to be discussed next, a cluster of three to five observations is typical as shown in Figure 13.

38
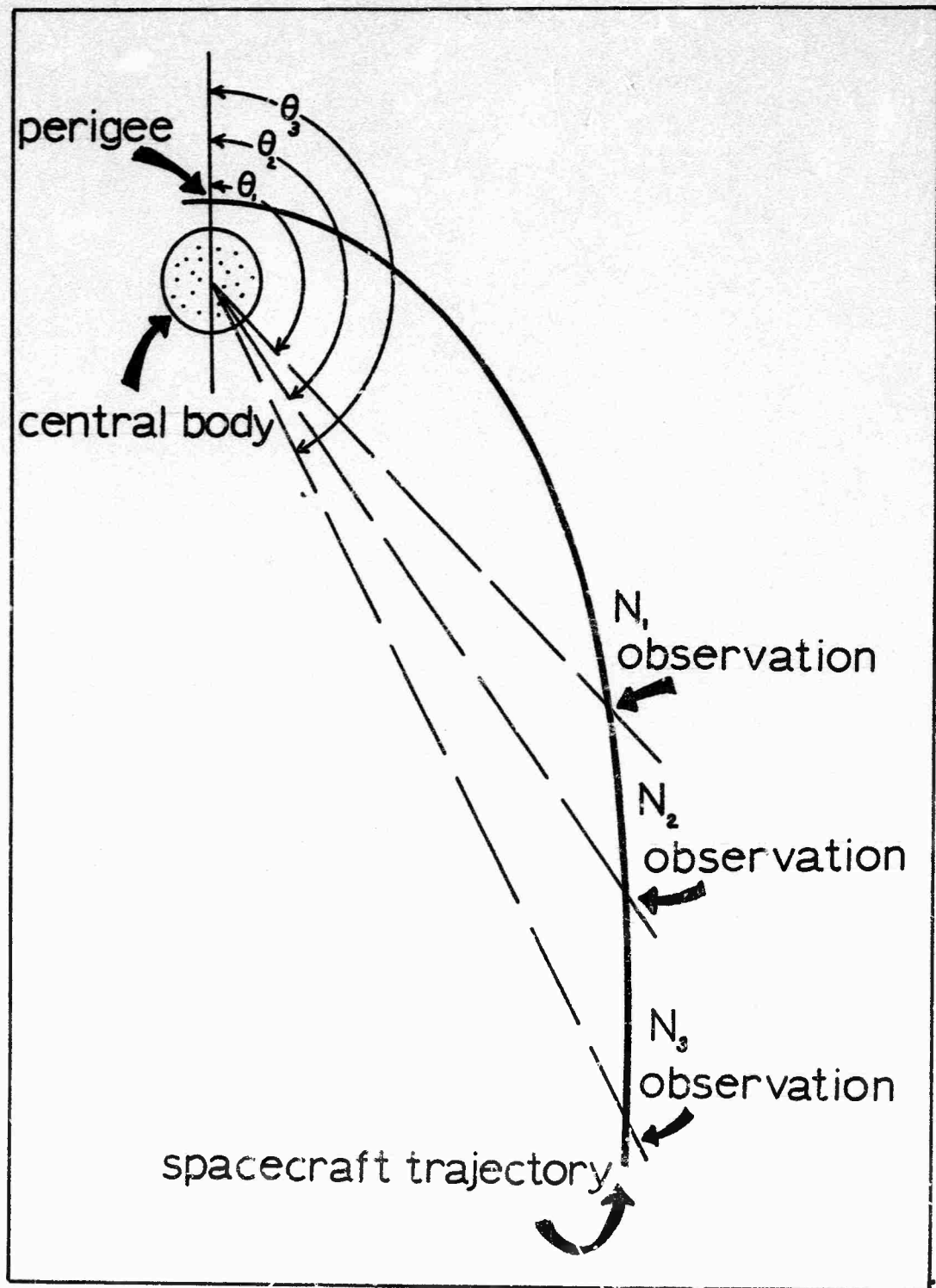
Figure 13.   Typical Trajectory with
Observation Schedule
(From Ref 15:24)

The central body in all cases discussed is the earth where the gravitational constant μ is 62750.717 NM^3/sec^2.

Sample Problem 1

Five LOP's have been established at 15 minute intervals and the great circle arcs separating each point has been calculated. Since angular differences are involved let $\psi_1 = 0$ degrees. The angular data is $\psi_1 = 0$, $\psi_2 = 6.464$, $\psi_3 = 12.787$, $\psi_4 = 18.992$, and $\psi_5 = 25.106$. In addition, one range sighting was obtained on the third observation; thus, $r_3 = 15,475$ NM

From the numerical differentiation formulas in Appendix B, the time derivatives of ψ_3 expressed in seconds are

$$\dot{\psi}_3 = \frac{-\left(\psi_5 - \psi_1\right) - 8\left(\psi_4 - \psi_2\right)}{12\,t}$$

$$= \frac{-25.106 + 8\left(12.58\right)}{12\left(900\right)}$$

$$= 69.6 \times 10^{-4} \quad deg/sec$$

$$= 1.215 \times 10^{-4} \quad rad/sec$$

and

$$\ddot{\psi}_3 = \frac{-\left(\psi_1 + \psi_5\right) + 16\left(\psi_2 + \psi_4\right) - 30\,\psi_3}{12\,t^2}$$

$$= \frac{-25.106 + 16\,(25.426) - 30\,(12.787)}{12\,(900)(900)}$$

$$= \frac{-0.106 + 16\,(0.456) - 30\,(0.287)}{12\,(900)(900)}$$

$$= -1.455 \times 10^{-7} \; deg/sec$$

$$= -2.56 \times 10^{-9} \; rad/sec$$

$$\dot{r} = -\frac{r\ddot{\theta}}{2\dot{\theta}} \qquad\qquad (3\text{-}26)$$

$$= -\frac{(1.5475 \times 10^{4})(-2.56 \times 10^{-9})}{2(1.215 \times 10^{-4})}$$

$$= 1.625 \times 10^{-1} \; NM/sec$$

$$X = \frac{r^{3}\dot{\theta}^{2}}{\mu} \qquad\qquad (3\text{-}8)$$

$$= \frac{(1.5475 \times 10^{4})^{3}(1.215 \times 10^{-4})^{2}}{6.275 \times 10^{4}}$$

$$= 8.75 \times 10^{-1}$$

$$Y = \frac{\dot{r}\,r^{2}\dot{\theta}}{\mu} \qquad\qquad (3\text{-}9)$$

$$= \frac{(1.625 \times 10^{-1})(1.5475 \times 10^{4})^{2}(1.215 \times 10^{-4})}{6.275 \times 10^{4}}$$

$$= 7.56 \times 10^{-2}$$

Plotting X, Y on the hodograph, Fig. 14, produces an eccen-
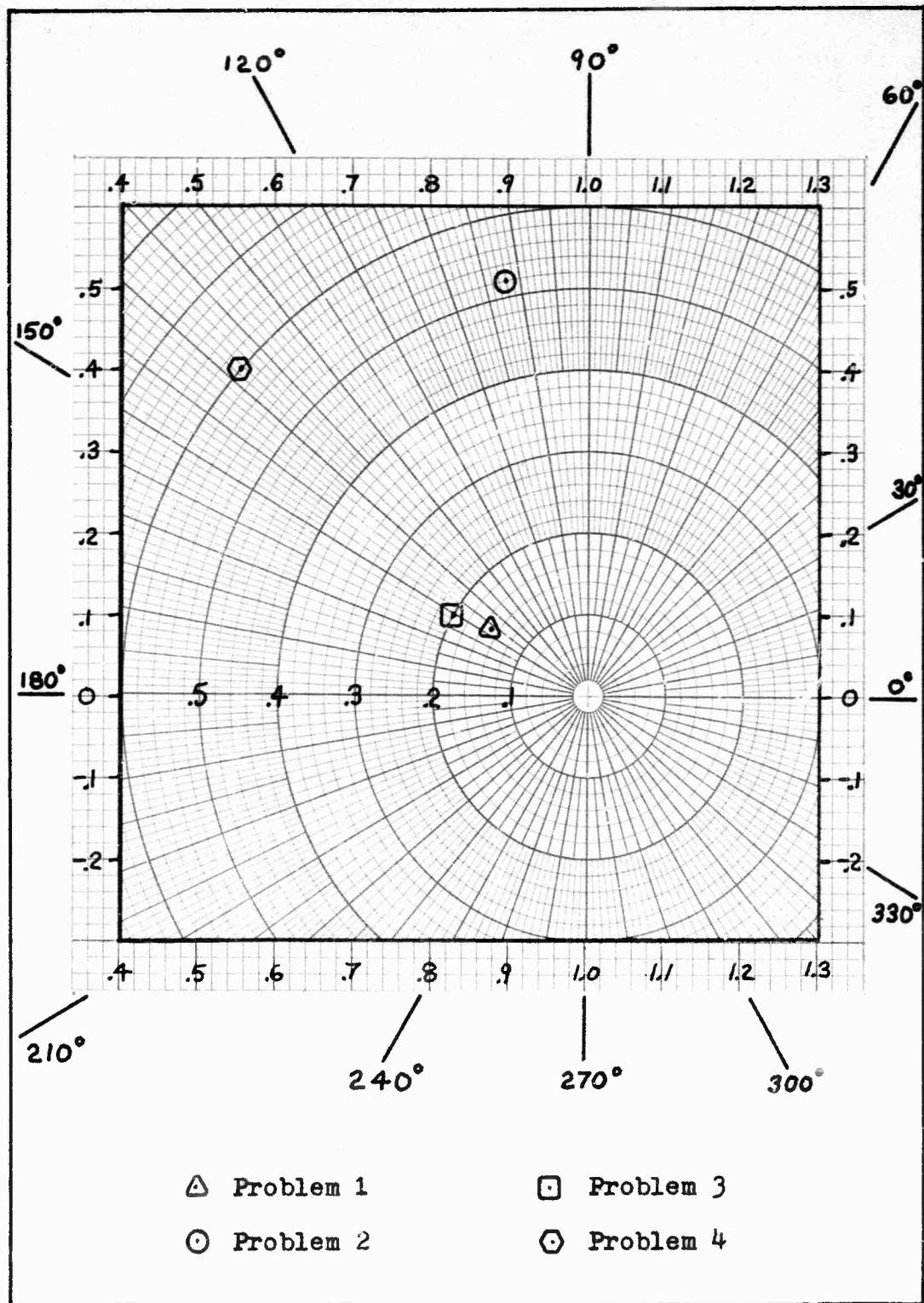
Figure 14. Partial Hodograph with Sample Problem Solutions

tricity of about .15 and a true anomaly of 148 degrees.
A more precise graph would have yielded

$$e = 0.1496$$
$$\theta = 147.5^\circ$$

$$a = \frac{r X}{1 - e^2} \qquad\qquad (3\text{-}21)$$

$$= \frac{(1.5475 \times 10^4)(8.75 \times 10^{-1})}{1 - (0.1496)^2}$$

$$= 13,830 \ NM$$

The exact values used in setting up the problem are

$$a = 13,760 \ NM$$
$$e = 0.15$$
$$\theta = 150.696^\circ$$

Sample Problem 2

Three range measurements separated by 15 minute intervals are obtained, but no LOP is established. The ranges expressed in nautical miles are $r_1 = 9896$, $r_2 = 11098$ and $r_3 = 12253$. Then from numerical differentiation

$$\dot{r}_2 = \frac{r_3 - r_1}{2t}$$

$$= \frac{12253 - 9896}{2(900)}$$

$$= 1.309 \ NM/sec$$

$$\ddot{r}_2 = \frac{r_1 + r_3 - 2r_2}{t^2}$$

$$= \frac{9896 + 12253 - 2(11098)}{(900)(900)}$$

$$= -5.8 \times 10^{-5} \ NM/sec^2$$

$$X = 1. + \frac{r^2 \ddot{r}}{\mu} \qquad (3\text{-}24a)$$

$$= 1. + \frac{(1.1093 \times 10^4)^2 (-5.8 \times 10^{-5})}{6.275 \times 10^4}$$

$$= 0.886$$

$$Y = \dot{r} \sqrt{\frac{rX}{\mu}} \qquad (3\text{-}25a)$$

$$= 1.309 \sqrt{\frac{(1.1098 \times 10^4)(0.886)}{6.275 \times 10^4}}$$

$$= 0.519$$

Plotting X,Y on Figure 14 appears to yield an eccentricity of 0.526 and 102° for true anomaly

$$a = \frac{rX}{1 - e^2} \qquad (3\text{-}21)$$

44

$$= \frac{(1.1098 \times 10^4)(0.886)}{1 - 0.526^2}$$

$$= 13,600 \ NM$$

The actual values used in this problem were

$$a = 13,760 \ NM$$
$$e = 0.5$$
$$\theta = 98.060^\circ$$

Sample Problem 3

The problem to be now considered is the situation where range data is not available for some unexplained reason. The angular data obtained over 20 minute intervals is $\theta_0 = 0^\circ$, $\theta_1 = 12.883^\circ$, $\theta_2 = 25.109^\circ$, $\theta_3 = 36.944^\circ$ and $\theta_4 = 48.657^\circ$. The angular velocities are found to be

$$\dot{\theta}_1 = 1.820 \times 10^{-4} \ \text{rad/sec}$$
$$\dot{\theta}_2 = 1.745 \times 10^{-4} \ \text{rad/sec}$$
$$\dot{\theta}_3 = 1.713 \times 10^{-4} \ \text{rad/sec}$$

Using Eq (3-29), (3-30), and (3-31) is somewhat laborious. In order to retain significant digits, a desk calculator was used to accomplish much more rapidly what could have been done otherwise by hand calculations. The results obtained were

$$\tilde{Q} = -2.5704 \times 10^{-5}$$

$$\tilde{R} = 1.5072 \times 10^{-5}$$

$$\tilde{S} = 1.4939 \times 10^{-4}$$

and from Eq (3-33) and (3-34)

$$X = .8279$$

$$Y = .1009$$

The range corresponding to position θ_i is

$$\tau_i = \left(\frac{\mu X}{\dot{\theta_i}^2} \right)^{1/3} \tag{3-35}$$

and yields a value for r_i of 11575 NM.

When X,Y is plotted on Figure 14 it appears to indicate an eccentricity of 0.2 and a true anomaly of 150°.

The actual values in setting up this problem are

$$e = 0.2$$
$$\theta_i = 150.658^o$$
$$r_i = 11,627 \text{ NM}$$
$$a = 10,000 \text{ NM}$$

Sample Problem 4

This last example represents the case where three complete position fixes are known. The data has been reduced to

$$r_1 = 11{,}489 \text{ NM} \qquad \psi_1 = 0^\circ$$

$$r_2 = 12{,}604 \text{ NM} \qquad \psi_2 = 7.541^\circ$$

$$r_3 = 13{,}619 \text{ NM} \qquad \psi_3 = 14.482^\circ$$

The equations to be used are

$$e \sin \theta_1 = \frac{\left[\dfrac{r_2 - r_1}{r_1 - r_2 \cos \psi_2}\right] - \left[\dfrac{r_3 - r_1}{r_1 - r_3 \cos \psi_3}\right]}{\left[\dfrac{r_2 \sin \psi_2}{r_1 - r_2 \cos \psi_2}\right] - \left[\dfrac{r_3 \sin \psi_3}{r_1 - r_3 \cos \psi_3}\right]} \qquad (E\text{-}8)$$

and

$$e \cos \theta_1 = \left[\frac{r_2 - r_1}{r_1 - r_2 \cos \psi_2}\right] - \left[\frac{r_2 \sin \psi_2}{r_1 - r_2 \cos \psi_2}\right] e \sin \theta_1 \qquad (E\text{-}9)$$

See Appendix E for derivation of the above formulas.
Breaking down Eq (E-8) into its basic terms yields

$$\frac{r_2 - r_1}{r_1 - r_2 \cos \psi_2} = \frac{12604 - 11489}{11489 - (12604)(0.99135)}$$

47

$$= \frac{1115}{-1005}$$

$$= -1.109$$

$$\frac{r_3 - r_1}{r_1 - r_3 \cos \psi_3} = \frac{13619 - 11489}{11489 - (13619)(0.96823)}$$

$$= \frac{2130}{-1707}$$

$$= -1.245$$

$$\frac{r_2 \sin \psi_2}{r_1 - r_2 \cos \psi_2} = \frac{(12604)(0.13124)}{-1005}$$

$$= -1.650$$

$$\frac{r_3 \sin \psi_3}{r_1 - r_3 \cos \psi_3} = \frac{(13619)(0.25008)}{-1707}$$

$$= -1.990$$

$$e \sin \theta_1 = \frac{-1.109 + 1.245}{-1.650 + 1.990}$$

$$= 0.400$$

$$e \cos \theta_1 = -1.109 - (-1.650)(0.400)$$

$$= -0.449$$

Therefore

$$X = 0.551$$

and

$$Y = 0.400$$

Plotting X,Y on Figure 14 produces an eccentricity of about 0.6 and a true anomaly of about 138 degrees. The semi-major axis is

$$a = \frac{rX}{1 - e^2} \tag{3-21}$$

$$= \frac{(11489)(0.551)}{1 - (0.6)^2}$$

$$\approx 10,000 \ NM$$

The actual values in this problem are

$$e = 0.6$$

$$\theta = 137.580^{\circ}$$

$$a = 10,000 \text{ NM}$$

Discussion

The sample problems were intended to show the reader that situations where the data is restricted in some form or other can be solved just as the theory indicates. Admittedly, the examples selected to demonstrate the various situations were chosen with care.

Sample problems 1, 2, and 3 rely on derivatives obtained through numerical differentiation and consequently contain truncation errors. Truncation errors are minimized as the time interval gets smaller. On the other hand, measurement errors are magnified by the numerical differentiation algorithms as the time interval gets smaller (Ref 17:97-98). All the sample cases selected consisted of range data correct to the nearest nautical mile and angular data correct to the nearest thousandth of a degree. Experimentation with time intervals of 5, 10, 15, 20, and 30 minutes and also experimentation with 3 and 5 point differentiation did not vary the results of eccentricity and semi-major axis by more than 2 per cent when a fixed position on the orbit was selected. By contrast, however, the point of the orbit selected for experimenta-

tion had an enormous effect. Had Sample Problem 2 been
set up with the same time interval but at the true anomaly
of 150° instead of 98°, the solution would have produced
an eccentricity of about 0.4 and a semi-major axis of
about 15,500 NM whereas the true values were 0.5 and
13,760 NM, respectively. Obviously this represents a
deviation which cannot be neglected, not even by the most
careless navigator. That approximate derivatives obtained
from finite differences should be viewed with skepticism
(Ref 17:97) seems to be good advice until some future
study reveals the criteria by which the end results ob-
tained through calculations involving numerical differen-
tiation can be accepted or rejected.

Sample Problem 4 consisting of three complete position
fixes does not rely on derivatives and not surprisingly
should yield an acceptable result always.

In Sample Problems 1 and 3, the shortcomings of try-
ing to retain significant digits through slide rule cal-
culations were quite evident to this author. To have
measuring instruments capable of measuring angles to the
thousandth of a degree and using five place trigonometric
tables but not being able to retain significant digits in
the calculations seems somewhat unreasonable. A hand-held
mechanical calculator such as the Curta Calculator which
is smaller than a four inch cube and weights less than one
pound yet has an eight significant figure accuracy (Ref 6:
167) appears to be a necessary item for any mission

requiring explicit manual navigation.

V. Ground Based Orbit Determination

Introduction

Since electrical navigational devices are barred from consideration in this thesis, the tracking of satellites must depend on optical means. In order to be visible, the spacecraft must carry its own light source or be illuminated by an external source such as the sun.

The optical sightings normally consist of angular measurements in azimuth and elevation taken from a "sensor" site local horizon.

Certain assumptions to be made are that

1. The coordinates of the site location are known.

2. The direction of planetocentric true "North" is known.

3. The true local vertical can be established.

4. The central body surface radius is known.

5. The central body rotation rate is known.

Simple Devices

The devices mentioned are crude devices in most instances and to a great extent resemble the schemes used by amateur moonwatchers.

The Mast

The mast is the simplest device. It consists of erecting a mast of known height with its longitudinal axis parallel to the local vertical. The ground about the site should be level to approximate a plane perpendicular to the local vertical.

The individual making the sightings must move about the mast in order to maintain the visible satellite's position just on top of the mast. As the individual tracks the satellite by moving his position about the mast, marking flags are dropped at recorded times. After satellite passage, the dropped flags can be used to directly establish azimuth and time. Knowing the observer's eyesight height and a little plane trigonometry can establish the angle of elevation (Ref 7:62). See Figure 15.

Slew Telescope

The slew telescope is essentially the most common instrument used to simultaneously provide a reading of azimuth and elevation. The principle is quite simple, featuring two degrees of freedom. In essence, the instrument consists of a sighting device mounted on a protractor which is free to swing on a pin connected to a vertical rotary shaft. A sketch is illustrated in Figure 16.

Techniques

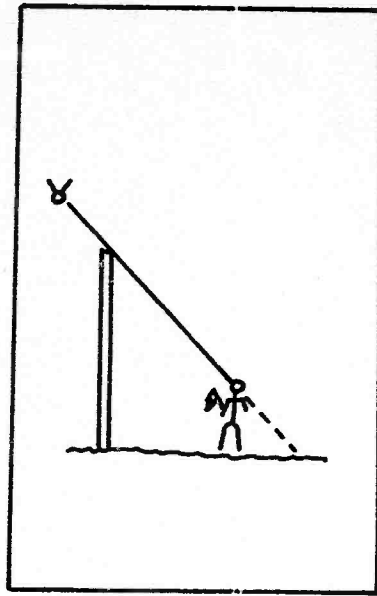In order to avoid using a laborious, classical orbit

Figure 15. The Mast
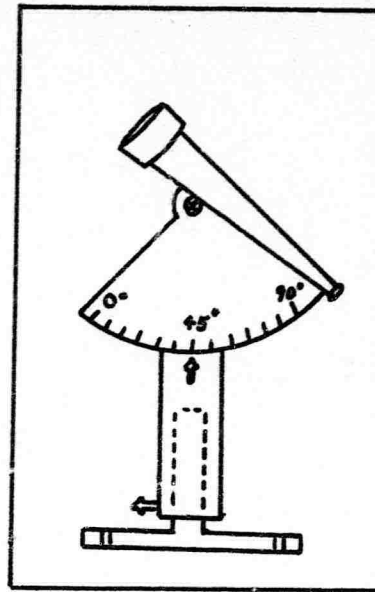
Figure 16. Slew
Telescope

determination scheme such as Laplace's Method, the slant

range to the target must be found to simplify calculations.

The methods used to find the range resort to triangulation,

but all triangulations require one known distance called

the baseline.

There are two basic techniques available. They are:

1. The two station-one pass method

2. The one station-two pass method.

The two station-one pass method can establish the

range to a satellite from only one satellite passage. The

baseline is the known separation distance between the two

stations. Due to restricted mobility, a mission landing

on some planet would not generally be expected to estab-
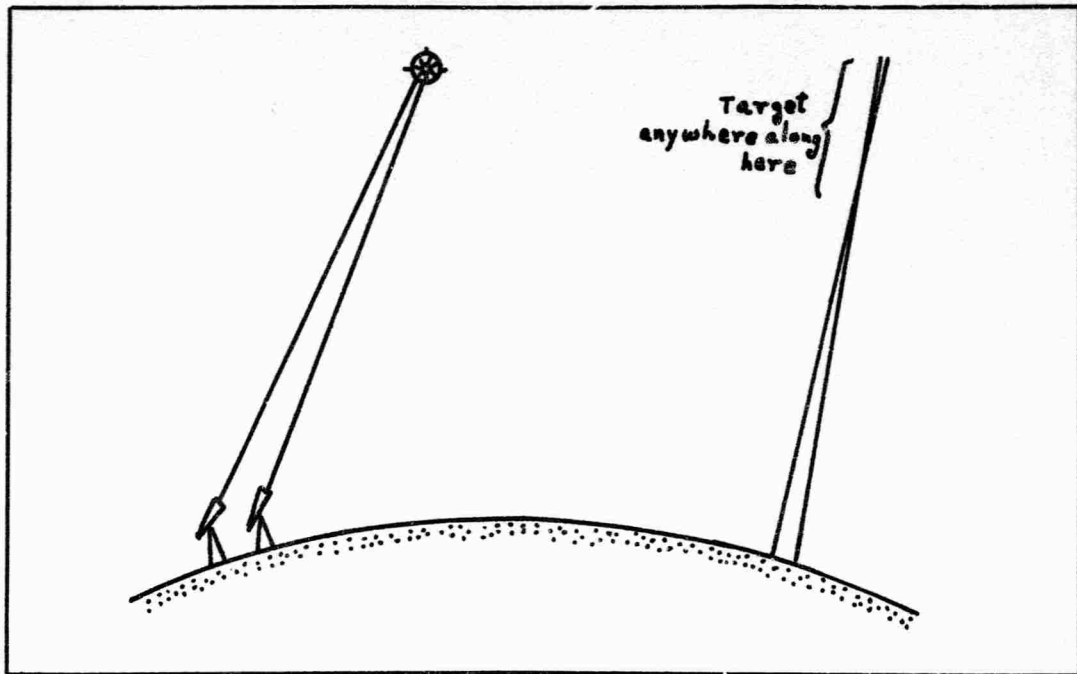
Figure 17.   Triangulation Error
(From Ref 11:121)

lish a long baseline. If the baseline is small compared
to the height of the target, the closing angle between the
two rays is extremely small, and slight tracking or mis-
alignment errors in the direction to the target will pro-
duce tremendous errors in range and spatial position to
the target (Ref 11:119-120). See Figure 17.

The one station-two pass method makes use of the
fact that an unperturbed orbital plane remains stationary
but due to the planet's rotation the sensor site has moved
its location with respect to that plane during the elapsed
time between satellite passage. The baseline is the chord
which separates the site locations with respect to the

orbital plane during each passage. Obviously the distance of the baseline is a function of angular rate of planet rotation and elapsed time. The time interval must correspond to the time between sighting the satellite on the first pass and sighting the satellite at the same position in its orbit on a succeeding pass. The baseline distance B can be expressed as

$$B = 2 R_b \cos \delta \sin \frac{\omega \Delta t}{2} \qquad (5\text{-}1)$$

where

R = body surface radius

δ = site latitude

ω = angular velocity of planet rotation

Δt = elapsed time

From the spherical isosceles triangle of Figure 18 it can be seen that the angles A_1 and $(360^o - A_2)$ must be equal and their magnitude is a function of Δt. With a precomputed table containing A_1 and A_2 versus values of Δt, a search of the tracking data can be made to find the azimuths A_1 and A_2 which will
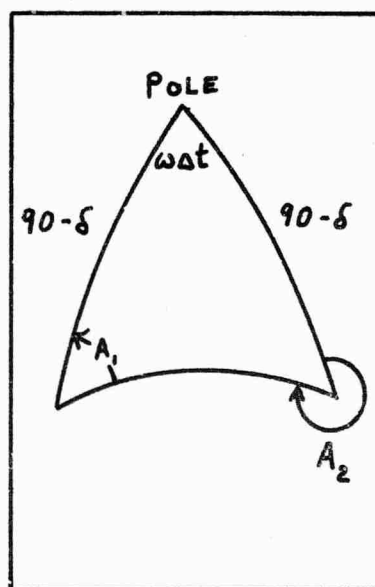

Figure 18. Azimuths Versus Elapsed Time

correspond to the elapsed time. The correct correspondence establishes a point on the orbit that is the common reference point between the two passages of the satellite.

The greatest difficulty arising from triangulation with the baseline is that the angle between the baseline and the satellite line-of-sight must be calculated through vector dot products. See Appendix F.

Satellite Position Fix

After calculating three slant ranges by triangulation, the satellite position can be determined quickly. The radial distance from body center to spacecraft is

$$r = R_b + r_s \sin(El) \qquad (5\text{-}2)$$

where

$$R_b = \text{body surface radius}$$
$$r_s = \text{slant range}$$
$$El = \text{elevation angle}$$

The great circle arc or angular ground distance ϕ from the site to the sub-satellite point is found from

$$\phi = \tan^{-1}\left[\frac{r_s \cos(El)}{R_b + r_s \sin(El)}\right] \qquad (5\text{-}3)$$
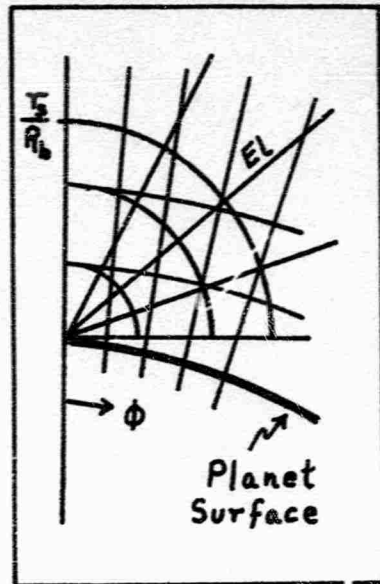
Figure 19

Range-Elevation Chart
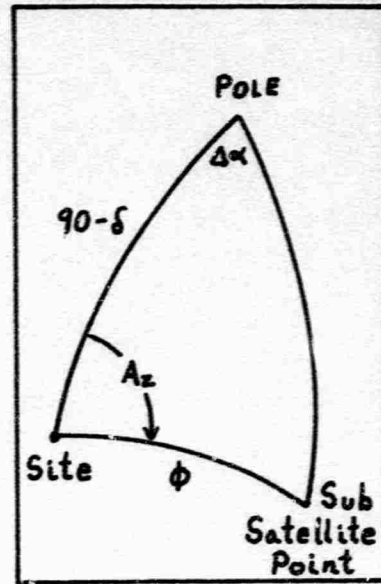
Figure 20

Geometry for
Sub-Satellite Point

An all-purpose non-dimensional chart such as illustrated
in Figure 19 can be used to obtain radial distance r and
angular ground distance ϕ.

Application of the sine and cosine laws of spherical
trigonometry allows one to calculate the position of the
sub-satellite point in terms of latitude and longitude
(See figure 20). Knowing the sub-satellite point is anal-
ogous to knowing the LOP in space navigation. From this
point on the solution is arrived at in the same manner as
Sample Problem 4 where three complete position fixes are
known.

Summary

The foregoing discussion merely served to show that satellite tracking does not differ greatly from space navigation. The tricky part concerns manipulation of the angular data to establish the slant range and then to determine the sub-satellite points. Once three satellite position fixes are known, the problem is solved in the same way as for space navigation where three complete position fixes are known.

VI. Conclusions and Recommendations

Introduction

This chapter comments on some of the impressions drawn from the research associated with this thesis. Under the subheading "Recommendations," some discussion of follow-on theses are briefly touched upon.

Conclusions

The following conclusions are offered as the result of experience gained in preparing this thesis:

1. Navigational devices which are simple in concept and design appear to present no problem from the theoretical point of view. The real problem arises when the instrument is integrated into a confined system which places restrictions on size, weight, and employment. Then, the simple device is transformed into a complex instrument requiring advanced and sophisticated engineering design; witness the transformation of the simple marine sextant to the complex space sextant.

2. The effects of oblateness on the range accuracy of stadimetric measurements involv-

ing devices viewing the entire target can be resolved by additional calculations. Thus, the accuracy in range is really dependent on how well the physical dimensions of a celestial body are known.

3. The composite graphs of the non-dimensional velocity hodograph appear to provide the navigator with a tool which can assist him in determining three orbital parameters (eccentricity, semi-major axis, and time to or from peripoint passage) plus the true anomaly. In addition to the fact that the velocity hodograph is a simple picture of any conical orbit, the hodograph has the potential of being used for guidance or orbital maneuvers which are usually the normal follow-up actions after determination.

4. Orbit determination can be completely or partially accomplished depending on what data is available by using first and second time derivatives of range and true anomaly obtained through numerical differentiation.

5. The accuracy of the geometric orbital parameters derived through numerical differentiation is more sensitive to the position of the spacecraft on its orbit than to the

time interval chosen.

6. Manual navigation aids such as a mechanical calculator is a necessity in order to retain the significant digits within the computations.

7. Ground level orbit determination is basically no different from on-board orbit determination. Without resorting to Laplace's Method or some similar scheme, the key to the problem's solution is determining range by triangulation so that three spatial fixes are obtained.

Recommendations

Some suggestions are offered for follow-on study topics. They are as follows:

1. Resolve the geometry of the stadimetric system viewing a limited portion of a non-spherical target.

2. Develop large size composite graphs of the velocity hodograph including a finely incremented constant time line graph and to investigate the handiness of the composite graphs thoroughly.

3. Investigate what criteria should be used to accept or reject the geometric orbital parameters obtained from calculations relying

63

on numerical differentiation when nothing is
originally known about the orbit.

Bibliography

1. Altman, Samuel P. Orbital Hodograph Analysis, Vol. III. Baltimore: American Astronautical Society Publication, 1965.

2. Bielkowicz, Peter. "Lecture Notes, Aerospace Trajectories, AE 5.61, AE 6.61, Chapter 6." Wright-Patterson Air Force Base, Ohio: Air Force Institute of Technology, 1967.

3. Boksenbom, Aaron S. Graphical Trajectory Analysis. NASA Technical Note No. D-64. Washington, D.C: National Aeronautics and Space Administration, 1959.

4. Chamberlin, James A. "Guidance Systems," in Manned Spacecraft Engineering Design and Operations. New York: Fairchild Publications, Inc., 1964.

5. Heacock, Frank A. Graphics in Space Flight. New York: Mc Graw-Hill Book Co., 1964.

6. Horrigan, Roger C., and Richard C. Walsh. Manual Astronaut Navigation. Unpublished Thesis. Wright-Patterson Air Force Base, Ohio: Air Force Institute of Technology, June 1969.

7. Howard, Neale E. Handbook for Observing the Satellites. New York: Thomas Y. Crowell Co., 1958.

8. Klass, Philip J. "Space Navigation Challenges Designers." Space Technology, 1:37-39 (July 1958).

9. Lampkin, B.A. and R.J. Randle. Investigation of a Manual Sextant-Sighting Task in the Ames Midcourse Navigation and Guidance Simulator. NASA Technical Note No. D-2844. Washington, D.C: National Aeronautics and Space Administration, 1965.

10. Lillestrand, R.L., and J.E. Carroll. "Horizon-Based Satellite Navigation Systems." IEEE Transactions on Aerospace and Navigational Electronics, 10:247-268 (September 1963).

11. Macko, Stanley J. Satellite Tracking. New York: John F. Rider Publisher, Inc., 1962.

12. McDonald William T., and Dr. Robert G. Stern. "Space Navigation." *Journal of the Institute of Navigation*, 14:416-433 (Winter 1967-68).

13. Mills, J.G., and Robert M. Silva. *Analytic Development of Optimum Astronaut Procedures for Use of the Air Force Space Navigation System in the Manual Mode*. Technical Report No. AFAL-TR-69-14. Wright-Patterson Air Force Base, Ohio: Air Force Avionics Laboratory, Research and Technology Division, 1969.

14. Moskowitz, S. "Sextants." *Navigation: Journal of the Institute of Navigation*, 12:194-199 (Autumn 1965).

15. Norvedt, Kenneth, Jr. *A Theory of Manual Space Navigation*. NASA Contractor Report No. CR-841. Washington, D.C: National Aeronautics and Space Administration, 1967.

16. Ordway, Frederick I., et al. *Applied Astronautics: An Introduction to Space Flight*. New York: Prentice Hall Co., 1963.

17. Scheid, F. *Schaum's Outline of Theory and Problems of Numerical Analysis*. New York: Mc Graw-Hill Book Co., 1968.

18. Schehr, Richard R., and Patrick J. Smith. *Manual Astronaut Navigation: Apollo Mission Applications*. Unpublished Thesis. Wright-Patterson Air Force Base, Ohio: Air Force Institute of Technology, June 1968.

19. Smith, Donald W. "Hand-Held Sextant: Results from Gemini XII and Flight Simulator Experiments." *Journal of Spacecraft and Rockets*, 5:655-661 (June 1968).

20. Smith, Donald W., and Bedford A. Lampkin. *Sextant Sighting Measurements from On-board the Gemini XII Spacecraft*. NASA Technical Note No. D-4952. Washington, D.C: National Aeronautics and Space Administration, 1968.

21. Sun, Fang Toh. "On the Hodograph Method for Solution of Orbit Problems," in *XIIth International Astronautical Congress, Washington, D.C., 1961 Proceedings*, Vol. II. New York: Academic Press Inc., 1963.

22. Szebehely, Victor G. *Progress in Astronautics and Aeronautics: Celestial Mechanics and Astrodynamics*, Vol. XIV. New York: Academic Press Inc., 1964.

23. Vorob'ev, L.M. *Spacecraft Navigation*. Jerusalem: Israel Program for Scientific Translations, 1966.

24. Walsh, Thomas K. <u>Factors Affecting the Design and Use of a Photographic Sextant for Space Navigation</u>. NASA Technical Note No. D-4285. Washington, D.C: National Aeronautics and Space Administration, 1967.

25. Webber, A., <u>et al</u>. <u>Space Position Fixing Techniques</u>, <u>Phase III a</u>. Technical Report No. APAL-TR-67-5. Wright-Patterson Air Force Base, Ohio: Air Force Avionics Laboratory, Research and Technology Division, 1967.

26. Weems, P.V.H. "Space Navigation," in <u>Post Apollo Space Exploration</u>. <u>Advances in the Astronautical Sciences</u>. Washington, D.C: American Astronautical Society Publication, 1966.

Appendix A

Supplementary Relationships in the Geometry of Stadimetric Measurement

The equations below (Ref 13:101) refer to Figure 5. The angle $\theta' - \delta\theta$ is measured; $\delta\theta$ is the correction angle due to the finite size of the center field of view.

Let $R = r_h$, then

$$\frac{\phi}{2} = \sin^{-1}\left\{\left[\frac{\frac{h}{R}\left(2+\frac{h}{R}\right)}{1-\left(\frac{1}{1+h/R}\right)^2}\right]^{\frac{1}{2}} \sin\frac{A}{2}\right\} \qquad (A-1)$$

$$\theta = \cos^{-1}\left\{\frac{\cos\frac{\phi}{2} + \cos^2\frac{A}{2}}{\cos\frac{A}{2}\left(1-\cos\frac{\phi}{2}\right)}\right\} \qquad (A-2)$$

$$\frac{\psi}{2} = \sin^{-1}\left\{\left[\frac{\frac{h}{R}\left(2-\frac{h}{R}\right)}{1-\left(\frac{1}{1-h/R}\right)^2}\right]^{\frac{1}{2}} \sin\frac{W}{2}\right\} \qquad (A-3)$$

$$\delta\theta = \cos^{-1}\left\{\frac{\cos\frac{\psi}{2} - \cos^2\frac{W}{2}}{\cos\frac{W}{2}\left(1-\cos\frac{\psi}{2}\right)}\right\} \qquad (A-4)$$

68

Appendix B

Numerical Differentiation Formulas

The first and second time derivatives are given below
for finite differences obtained from three to five read-
ings.

3 readings:

$$\dot{x}_2 = \frac{x_3 - x_1}{2t} \tag{B-1}$$

$$\ddot{x}_2 = \frac{x_1 + x_3 - 2x_2}{t^2} \tag{B-2}$$

4 readings:

$$\dot{x}_2 = \frac{3(2x_3 - x_2) - (2x_1 + x_4)}{6t} \tag{B-3}$$

$$\ddot{x}_2 = \frac{x_1 + x_3 - 2x_2}{t^2} \tag{B-4}$$

69

5 readings:

$$\dot{x}_3 = \frac{(x_1 - x_5) - 8(x_2 - x_4)}{12\,t} \qquad \text{(B-5)}$$

$$\ddot{x}_3 = \frac{-(x_1 + x_5) + 16(x_4 + x_2) - 30\,x_3}{12\,t^2} \qquad \text{(B-6)}$$

Appendix C

Radial Acceleration

When a body is in an exact circular motion it may be said that the centripetal acceleration is balanced by the gravitational acceleration in which case the radius is constant implying that $\dot{r} = \ddot{r} = 0$. Thus

$$r \dot{\theta}_{Lc}^2 = g \tag{C-1a}$$

or

$$V_{Lc}^2 = \left(r \dot{\theta} \right)^2 = g r \tag{C-1b}$$

where   g is the local gravitational acceleration at dis-
tance r

$\dot{\theta}_{Lc}$ is the local circular angular velocity

V_{Lc} is the local circular velocity

When $\dot{\theta} \neq \dot{\theta}_{Lc}$, the accelerations are not in balance;
and, there exists a radial acceleration $\ddot{r}$ and consequently
a radial velocity $\dot{r}$. The velocity is expressed as

$$V^2 = \left(r \dot{\theta} \right)^2 + \dot{r}^2 \tag{C-2}$$

71

and the relationship for radial acceleration as

$$r\dot{\theta}^2 = g + \ddot{r} \tag{C-3a}$$

or

$$\left(r\dot{\theta}\right)^2 = gr + r\ddot{r} \tag{C-3b}$$

Substituting Eq (C-1b) into (C-3b) yields

$$\left(r\dot{\theta}\right)^2 = \left(r\dot{\theta}_{LC}\right)^2 + r\ddot{r} \tag{C-4a}$$

or

$$\left(r\dot{\theta}\right)^2 = V_{LC}^2 + r\ddot{r} \tag{C-4b}$$

Appendix D

Orbital Orientation Parameters

It is assumed that two lines of position have been identified in terms of α and δ. The most general equations for the orientation parameters (Ref 10:265) are given below.
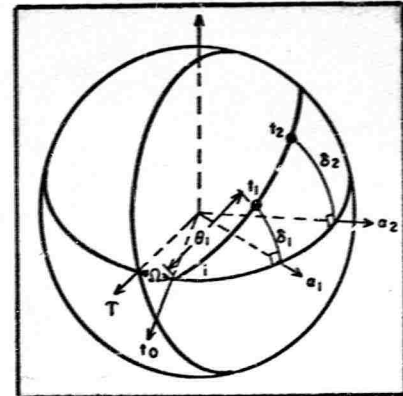

Figure 21
Three Dimensional
Geometry of an Orbit

Right ascension, Ω:

$$\Omega = \tan^{-1}\left\{\frac{\dfrac{\tan\delta_2}{\tan\delta_1}\sin\alpha_1 - \sin\alpha_2}{\dfrac{\tan\delta_2}{\tan\delta_1}\cos\alpha_1 - \cos\alpha_2}\right\} \qquad (D-1)$$

Inclination, i:

$$i = \tan^{-1}\left[\frac{\tan\delta_1}{\sin(\alpha_1 - \Omega)}\right] \qquad (D-2)$$

The true anomaly angle between the reference plane and point 1 is given by

$$\theta_i = \sin^{-1}\left[\frac{\sin \delta_i}{\sin i}\right] \qquad (D\text{-}3)$$

from which the argument of peripoint is

$$\omega = \theta_i - \theta_i \qquad (D\text{-}4)$$

where θ_i is the true anomaly at point 1 as obtained from the velocity hodograph.

Appendix E

Geometric Parameters from Range and Angle Data

This method can be used to find X and Y for the velocity hodograph when three complete position fixes are known. Since the LOP's of the position fixes are expressed in terms of latitude δ and longitude α, the great circle arcs connecting LOP's with the LOP of position fix 1 form spherical triangles where the two sides ($90^\circ - \delta_1$ and $90^\circ - \delta_i$) and the included polar angle ($\alpha_i - \alpha_1$) are all known. As defined here, the great circle arc of LOP 1 is a special case and may simply be expressed as

$$\psi_1 = 0 \tag{E-1}$$

The succeeding great circle arcs may be found from the law of cosines, thus

$$\psi_i = \cos^{-1}\left[\cos(90 - \delta_1) \cos(90 - \delta_i) \right.$$
$$\left. + \sin(90 - \delta_1) \sin(90 - \delta_i) \cos(\alpha_i - \alpha_1) \right] \tag{E-2}$$

which can be simplified to

$$\psi_i = \cos^{-1}\left[\sin\delta_1 \sin\delta_i + \cos\delta_1 \cos\delta_i \cos(\alpha_i - \alpha_1) \right] \tag{E-3}$$

75

It is evident that the time separation between fixes is immater'al in the above.

From the general polar equation of a conic trajectory

$$r\left(1 + e\cos\theta\right) = constant \qquad (E-4)$$

therefore let

$$r_1\left(1 + e\cos\theta\right) = r_2\left(1 + e\cos\left(\theta + \psi_2\right)\right) \qquad (E-5)$$

and

$$r_1\left(1 + e\cos\theta\right) = r_3\left(1 + e\cos\left(\theta + \psi_3\right)\right) \qquad (E-6)$$

Solving simultaneously by making use of the trigonometric identity

$$\cos\left(\theta + \psi\right) = \cos\theta\cos\psi - \sin\theta\sin\psi \qquad (E-7)$$

yields

$$e\sin\theta_1 = \frac{\left[\dfrac{r_2 - r_1}{r_1 - r_2\cos\psi_2}\right] - \left[\dfrac{r_3 - r_1}{r_1 - r_3\cos\psi_3}\right]}{\left[\dfrac{r_2\sin\psi_2}{r_1 - r_2\cos\psi_2}\right] - \left[\dfrac{r_3\sin\psi_3}{r_1 - r_3\cos\psi_3}\right]} \qquad (E-8)$$

76

and

$$e \cos \theta_1 = \left[\frac{r_2 - r_1}{r_1 - r_2 \cos \psi_2} \right] - \left[\frac{r_2 \sin \psi_2}{r_1 - r_2 \cos \psi_2} \right] e \sin \theta_1 \qquad \text{(E-9)}$$

Although Eq (E-8) and (E-9) look long, the calculations in Eq (E-8) are simple and straightforward; and, the terms of Eq (E-9) are repetitions of terms in Eq (E-8). Note that

$$X = 1 + e \cos \theta_1 \qquad \text{(3-10)}$$

and

$$Y = e \sin \theta_1 \qquad \text{(3-11)}$$

are the arguments for the velocity hodograph.

Appendix F

Baseline to Line-of-Sight Angle (σ)

To find the slant range along the line-of-sight one must know the angle formed between the baseline and line-of-sight before triangulation can be made with the baseline distance. A coordinate system is established such as illustrated in Figure 22.

The line-of-sight unit vector can be expressed as

$$\bar{1}_{LOS} = \cos(A_z)\cos(El)\,\bar{x} - \sin(A_z)\cos(El)\,\bar{y} + \sin(El)\,\bar{z} \qquad (F-1)$$
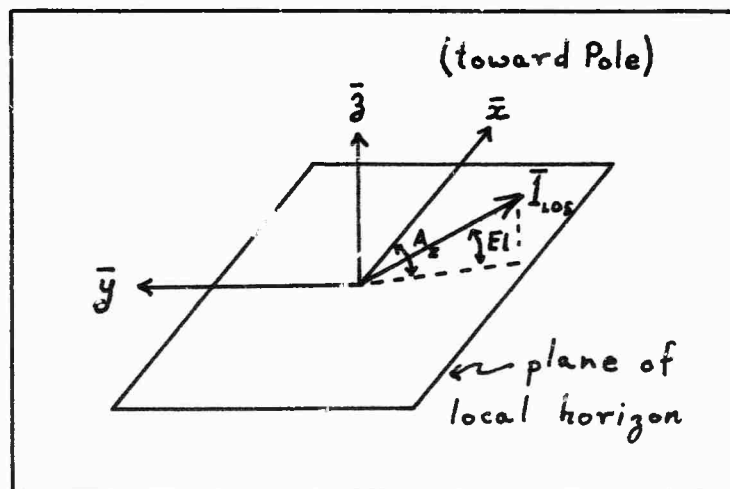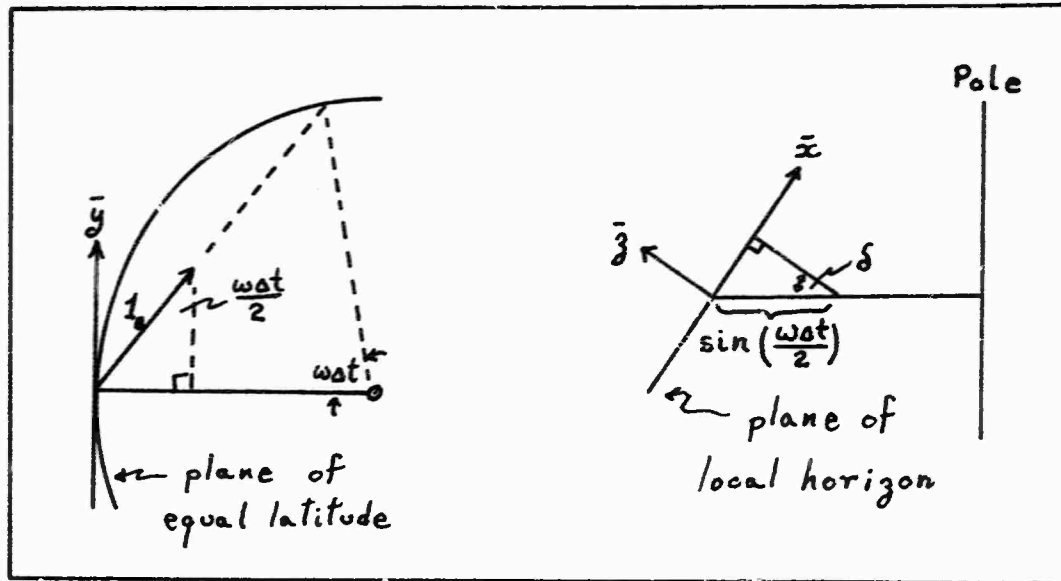
Figure 22
Line-of-Sight Unit Vector

Figure 23. Baseline Unit Vector

The baseline unit vector must also be expressed in terms of $\hat{x}, \hat{y}, \hat{z}$. From Figure 23, it can be seen that the baseline unit vector can be expressed as

$$\bar{1}_B = \sin\delta\,\sin\left(\frac{\omega_\Delta t}{2}\right)\hat{x} \pm \cos\left(\frac{\omega_\Delta t}{2}\right)\hat{y} - \cos\delta\,\sin\left(\frac{\omega_\Delta t}{2}\right)\hat{3} \quad (F-2)$$

where the sign of the term containing $\hat{y}$ depends on which end of the baseline one is making the calculations. (As drawn in Fig. 23 the sign is +.)

The angle σ between the baseline and the line-of-sight is

$$\sigma = \cos^{-1}\left[\bar{1}_{LOS} \cdot \bar{1}_B\right] \quad (F-3)$$

79

VITA

Daniel Henri Jean was ████████ █ ████████████████
██, ██ █████. He graduated from █████████████████
███████ Tampa, Florida in 1956 and entered the United
States Naval Academy at Annapolis, Maryland. He graduated
with a Bachelor of Science degree and received a regular
commission in the USAF in June 1960. He served as a Deputy
Missile Combat Crew Commander in the ICBM-Atlas complexes
of the 566th Strategic Missile Squadron, Francis E. Warren
Air Force Base, Wyoming. Subsequent assignments were
within the Space Defense System where he served as Special
Events Officer with the 1st Aerospace Control Squadron,
Ent Air Force Base, Colorado; and as Space Surveillance
Officer with the 2nd Surveillance Squadron (Detachment 1),
Shemya, Alaska and then with the 20th Surveillance Squad-
ron, Eglin Air Force Base, Florida until his entry into
the Air Force Institute of Technology.

Permanent address: ███████████████

This thesis was ████████████████ ███

DOCUMENT CONTROL DATA - R & D

(Security classification of title, body of abstract and indexing annotation must be entered when the overall report is classified)

1. ORIGINATING ACTIVITY (Corporate author)	2a. REPORT SECURITY CLASSIFICATION
Air Force Institute of Technology Wright-Patterson AFB, Ohio 45433	Unclassified
	2b. GROUP

3. REPORT TITLE

Methods and Design of Simple Devices for On-board and Ground-bound Orbit Determination

4. DESCRIPTIVE NOTES *(Type of report and inclusive dates)*

AFIT Thesis

5. AUTHOR(S) *(First name, middle initial, last name)*

Daniel H. Jean
Major   USAF

6. REPORT DATE	7a. TOTAL NO. OF PAGES	7b. NO. OF REFS
June 1971	88	26

8a. CONTRACT OR GRANT NO.	9a. ORIGINATOR'S REPORT NUMBER(S)
b. PROJECT NO.	GA/MC/71-1
c.	9b. OTHER REPORT NO(S) *(Any other numbers that may be assigned this report)*
d.	

10. DISTRIBUTION STATEMENT

Approved for public release, distribution unlimited.

11. SUPPLEMENTARY NOTES	12. SPONSORING MILITARY ACTIVITY
Approved for public release; IAW AFR 190-17 Jerry C. Hix, Captain, USAF Director of Information	

13. ABSTRACT

Simple non-electrical methods and devices for orbit determination on the basis of explicit navigation are examined. Principal measuring devices discussed are the sextant, stadimetric instruments, and almu-cantars. Computational methods for solving the geometric orbital parameters are focused on adaptations of the velocity hodograph. Discussion includes sample problems and a general analysis of inherent errors.

DD FORM 1 NOV 65 **1473**